U.PORTO
FEUP FACULDADE DE ENGENHARIA
UNIVERSIDADE DO PORTO
M 2022

PRODUCTION OF A SAE H13 MOULD INSERT BY HOT EMBOSSING AND A BRIEF COMPARISON WITH THE MATERIAL EXTRUSION AM PROCESS

FERNANDO YE LIN

DISSERTAÇÃO DE MESTRADO APRESENTADA
À FACULDADE DE ENGENHARIA DA UNIVERSIDADE DO PORTO EM SETEMBRO DE 2022

ORIENTADORA

ELSA WELLENKAMP DE SEQUEIROS

CANDIDATO	Fernando Ye Lin	*Código*	201604569
TÍTULO	Production of SAE H13 mould insert by hot embossing and a brief comparison with the material extrusion AM process		
DATA	16 de setembro de 2022 – 16 h 00		
LOCAL	FEUP/DEMM – sala F107		

JÚRI	Presidente	José Carlos Magalhães Duque da Fonseca	DEMM/FEUP
	Arguente	Omid Emanidinia	INEGI
	Orientadora	Elsa Wellenkamp de Sequeiros	DEMM/FEUP

“人往高处走，水往低处流”

A Chinese popular saying

Abstract

Currently, hot embossing is a very appealing replication technology for the production and replication of polymeric microstructures. Over the years, the scientific community has studied the feasibility of its application in mixtures of metal powders and polymeric binders to manufacture metallic components. The general approach has followed the following sequence: raw material production, hot embossing, removal of the polymeric binder (debinding) and sintering.

However, within the technologies involving metal powders, there is a set of contending technologies that have attracted tremendous attention from researchers: additive manufacturing (AM). Additive manufacturing is a disruptive and innovative process. It is a technology that displays a massive potential to manufacture metallic components with complex geometries. This fact leads us to question whether the AM may come to make the research of the powder hot embossing technology obsolete. In this sense, this work arises as an attempt to elucidate the question raised through the faithfulness of details of a given geometry produced by the two technologies (micro hot embossing and AM).

The methodology employed in this work will have the following sequence: a study of multiple temperatures, pressure and holding time conditions in the micro hot embossing of two powders and binder mixtures (SAE H13:M1 and a SAE H13 filament used in material extrusion); assessment of the final results (details and mechanical properties) of components and compared it with the same geometry produced in additive manufacturing technology (material extrusion). For this purpose, the raw materials such as SAE H13 powder, M1 binder and filament were characterised and prepared for the shaping stage. The bulking of the components obtained in both processes (hot micro hot embossing and material extrusion) carried through thermal cycles of binder removal and sintering. Finally, these components obtained were visually inspected and mechanically characterised.

From the results obtained, it can be seen that the best hot embossing replication conditions were 220 ºC/8 MPa/ 45 minutes and 210 ºC/8 MPa/ 30 minutes for SAE H13:M1 and filament blends, respectively. As for the component produced by AM, the replication was, unfortunately, mediocre compared to the relative success obtained in hot embossing. This observation leads us to conclude that micro hot embossing preserves, for the time being, its value as a viable powder metallurgy process for microdetail replication.

Resumo

Atualmente, a gravação a quente é uma tecnologia replicativa bastante atrativa para a produção e replicação de microestruturas poliméricas. Ao longo dos anos, a comunidade científica tem estudado a viabilidade da sua aplicação em misturas de pós metálicos e ligante polimérico, para a produção de componentes metálicos. A abordagem, de um modo geral, tem seguido a seguinte sequência: produção da matéria-prima; conformação a quente; remoção do ligante polimérico e sinterização.

Contudo, dentro das tecnologias envolvendo pós metálicos, existe um conjunto de tecnologias concorrentes que têm atraído grande atenção dos investigadores: a manufatura aditiva (MA). A manufatura aditiva é um processo disruptivo, inovador e demonstra imenso potencial para a produzir componentes metálicos de geometrias complexas. Isto leva-nos a questionar se a MA pode vir a tornar a investigação da tecnologia de gravação a quente de pós, obsoleta. Nesse sentido, este trabalho surge como uma tentativa de elucidar a questão levantada, através de uma comparação da fidelidade de replicação de detalhes de uma determinada geometria entre as duas tecnologias (microgravação a quente e MA).

A metodologia deste trabalho seguirá a seguinte sequência: estudar várias condições de temperatura, pressão e tempo na microgravação a quente de duas misturas de pó:ligante (SAE H13:M1 e um filamento de SAE H13 utilizado em extrusão de material); avaliação do resultado final (detalhes e propriedades mecânicas) dos componentes e a sua comparação com a mesma geometria produzida numa tecnologia de manufatura aditiva (extrusão de material). Para tal, as matérias-primas como o pó de SAE H13, ligante M1 e filamento foram caracterizadas e preparadas para serem posteriormente submetidas à etapa de conformação. A consolidação dos componentes obtidos em ambos os processos (microgravação a quente e extrusão de material) deu-se com recurso a ciclos térmicos de remoção de ligante e sinterização. Por fim, os componentes obtidos foram inspecionados visualmente e caracterizados mecanicamente.

Dos resultados obtidos, constata-se que as melhores condições de replicação de gravação a quente foram de 220 ºC/8 MPa/ 45 minutos e 210 ºC/8 MPa/ 30 minutos para as misturas SAE H13:M1 e filamento, respetivamente. Quanto ao componente produzido por MA, a replicação foi infelizmente medíocre comparado com o relativo sucesso obtido na microgravação a quente. Isto leva-nos a concluir que a microgravação a quente preserva, por enquanto, o seu valor como um processo viável de pulverometalurgia para a replicação de microdetalhes.

Agradecimentos

Em primeiro lugar, gostaria de agradecer à minha orientadora Prof. Elsa Sequeiros por me ter orientado nestes meses de trabalho, por esclarecer sempre as minhas dúvidas.

Agradeço ao Engenheiro Europeu José Costa por me ter fornecido matéria-prima essencial para a execução do meu trabalho e à Prof. Aida Moreira pela ajuda na manipulação do forno.

Quero agradecer à minha família e em particular aos meus irmãos que foram fundamentais nos momentos em que me sentia desmotivado. Agradeço-vos pelo companheirismo, pelas discussões pertinentes e pelas conversas *random* que me faziam esquecer por um bocado as preocupações que ia tendo ao longo desta jornada. Agradeço ao Filipe que me acompanhou durante todo o meu percurso académico e tornou estes cinco anos mais agradáveis de percorrer.

Agradeço aos meus amigos, colegas e em particular à Elsa que demonstrou ser uma colega e amiga excecional.

Agradeço aos restantes professores que contribuíram de alguma forma para o sucesso do meu percurso académico.

Não me poderia esquecer de agradecer ao Sr. Ramiro e à D. Cândida que se mostraram disponíveis para me fornecer auxílio e materiais.

Index

Figure Index

Table index

Abbreviations

CAD	Computer Aided Design
CSL	Critical Solid Loading
DOE	Design Of Experiments
DSC	Differential Scanning Calorimetry
DMD	Direct Metal Deposition
DED	Directed Energy Deposition
EBMa	Electron Beam Machining
EBM	Electron Beam Melting
LPBF	Laser Powder Bed Fusion
ME	Material Extrusion
µ-PIM	Micro Powder Injection Mouding
PW	Paraffin Wax
PSD	Particle Size Distribution
PP	Polypropylene
PBF	Powder Bed Fusion
PIM	Powder Injection Moulding
PL	Powder Loading
SA	Stearic Acid
TGA	Thermogravimetric Analysis
UTS	Ultimate Tensile Strength
YS	Yield Strength

1. Introduction

The reproduction and the quality of details in a final component are essential in the plastic industry, namely in injection moulding. Modifying small pieces in a final product would imply a readjustment in the mould used or the production of a new mould with the intended amendments [1]. To circumvent the aspects above, it is interesting to use metal inserts that can be inserted in specific locations of a mould. The ease of adding inserts into a mould offers a degree of customisation that would not be possible with conventional moulds. However, the inserts may have complicated details and geometries, so appropriate manufacturing processes are required to produce them [1].

The shaping process to obtain the desired geometry is usually achieved by micro-machining (adaptation of the conventional machining method to the micro-scale) or electron beam machining (EBMa). However, micro-machining and EBMa are time-consuming and somewhat expensive technologies [2].

The production of metallic components by powder metallurgy is an alternative to conventional manufacturing processes that invariably start from bulk material. Although the production of components through powder-based technologies has less expression when compared with conventional ones, it exhibits several advantages. Powder metallurgy is not truly demanding in terms of labour and energy, generates little raw material waste, is ecologically utterly clean, and is a technology capable of producing intricate components with properties comparable to bulk components [3].

Currently, when we mention the subject of powder metallurgy, one of the first and most promising and disruptive technologies for manufacturing complex geometries is additive manufacturing (AM). AM is a layer-by-layer production process with an inherently high degree of design freedom that allows the design of parts impossible to produce by any other manufacturing process (other powder metallurgy techniques or subtractive processes) [3].

Other powder-based technologies include, for example, powder injection moulding (PIM) or, recently, metal powder hot embossing. Although the hot embossing of metal powders has not yet been on an industrial-scale application, efforts are being made to broaden the knowledge on the subject [4].

In the scope of this work, we intend to study the processing conditions of hot embossing of a tool steel powder, its feasibility in the production of an insert and replication of the micrometric details. Simultaneously, we intend to make a comparative analysis with an additive manufacturing process and to evaluate the degree of detail faithfulness, and the drawbacks of both methods.

The state-of-the-art for this work will start by describing the hot embossing process and all its associated steps. It will culminate in a generalised approach to additive manufacturing processes with a particular emphasis on fused filament fabrication.

2. State of the art

2.1. Powder hot embossing

Hot embossing is a non-injection-based replication technology that replicates a microstructured master (as a mould insert) in a component. Replication of microstructures by embossing is not something completely innovative. Although it is unimaginable to compare it with the high-aspect structures obtainable today, it is possible to see traces of this technology in the past [5].

An obvious example is the embossing of coins in ancient civilisations. Although the engravings on these coins have relatively small-scale details, these did not reach micrometric dimensions due to a lack of dedicated technological equipment. Nonetheless, the engraving of micrometric details backdates to the middle of the 20th century to produce micro-grooves on vinyl music records (Figure 1) [5].

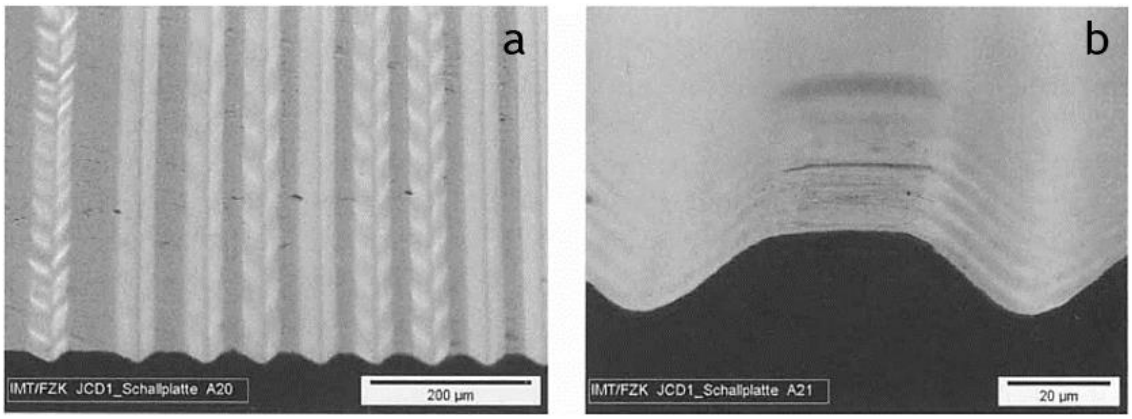

Figure 1: SEM images of the a) micro-grooves in the vinyl music records and b) detailed view [5].

Hot embossing technology is well established in the polymeric industry. This engraving process distinguishes four key stages (Figure 2) [6]:

I. Heating the tool and the substrate on which a semi-finished product is placed and fixed. This polymeric product is heated until it reaches the moulding or glass transition temperature.
II. Keeping the temperature constant, the mould containing the insert is pressed against the semi-finished product. This step occurs under a vacuum atmosphere to minimise the possibility of air bubbles incorporation, and then the embossing pressure and displacement are controlled. Note that the thickness of the product must be greater than the depth of the deepest cavity of the insert.
III. Cooling of the system below the moulding temperature without pressure relieving. The exerted pressure avoids the backflow of the material before it is rigid.
IV. Demoulding of the component by pulling away from the substrate and tool. This step is critical. Depending on various factors (insert design, tool quality, release force), and

in extreme cases, the release may be impossible, resulting in damage to both the insert and the final product.

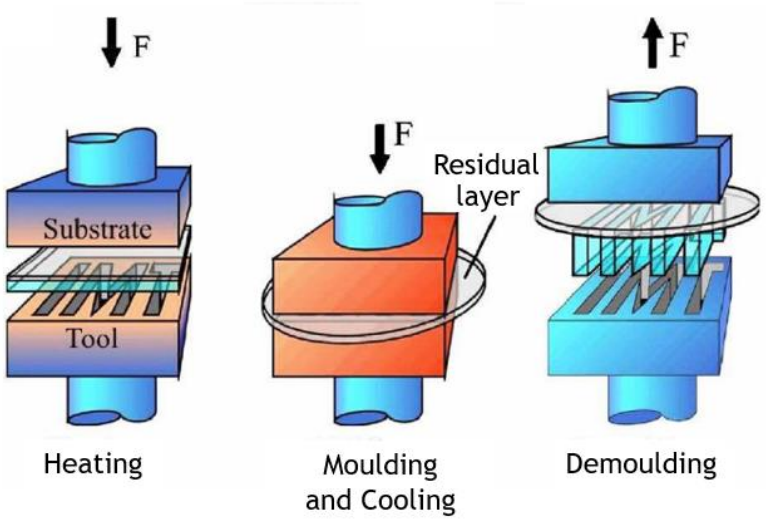

Figure 2: Schematic representation of different hot embossing stages [6].

As previously stated, the application of hot embossing in powder systems is a subject that is still under development. To produce metallic components using the metal powder hot embossing technology, four fundamental steps can be distinguished (Figure 3):

I. Production of a feedstock;
II. Hot embossing (shaping with the application of pressure and adequate temperature);
III. Binder removal (debinding);
IV. Solid state sintering.

The procedure for the hot embossing of metallic powders presents similarities with the methodology applied to the microinjection of metallic powders (μ-PIM). The hot embossing of metallic powders is, bluntly saying, a technology inspired by the μ-PIM by just modifying the shaping step [7,8].

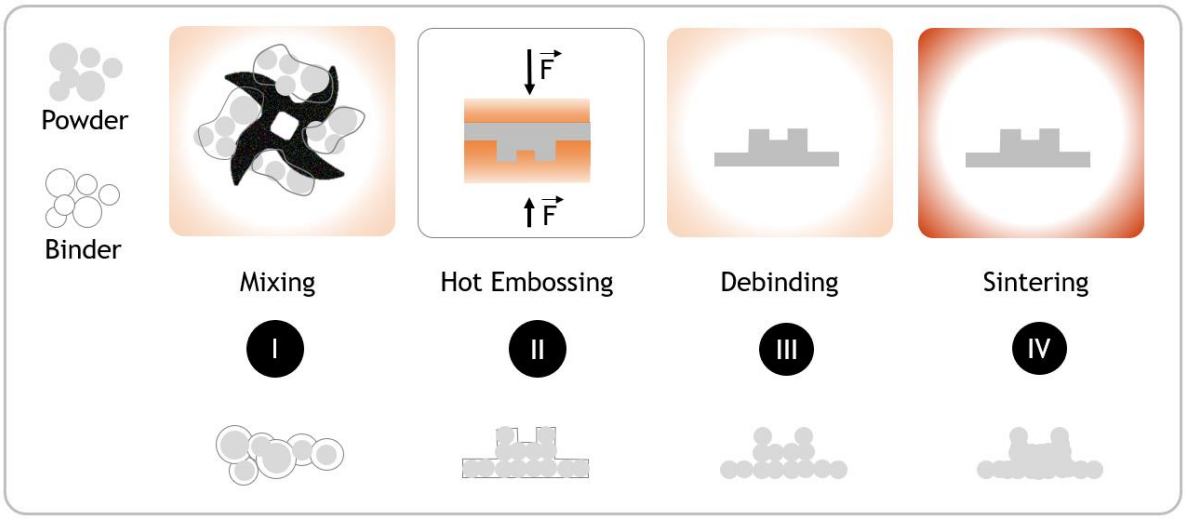

Figure 3: Illustration of the main steps of hot embossing. Adapted from [8].

2.1.1. Selection of the powder-binder pair and preparation of a feedstock

Like any manufacturing process, it is mandatory to have materials with the appropriate characteristics for the process in question. In the case of the hot embossing of metallic powders, the component is produced with a feedstock material. Similarly to the μ-PIM, the feedstock of hot embossing consists of a mixture of a metallic powder and polymeric binder in specific proportions [9].

Defining the optimal ratio of the powder-binder pair is critical to successfully producing small components with intricate details. It is important to note that proper mixing and dispersion of the powder in the binder are crucial steps to obtaining a homogeneous feedstock without agglomeration and porosity. So, the particles should have a thin layer of binder cover [9,10].

In the powder-binder system, the metal powder is a component of the mixture ubiquitously present during the entire process. The powder particles must exhibit constant physicochemical characteristics to ensure replicability, like in any manufacturing process. The most important aspects of a powder are its morphology (ideally spherical) and a particle size distribution that allows the best packing and maximum densification. It is possible to highlight other factors equally relevant to the rheology of powders, such as density, moisture, chemical composition, flowability, specific surface area, compressibility, sintering suitability and thermal properties [11]. To the best of the author's knowledge, to date, the most studied powder for hot embossing seems to be the SAE 316L stainless steel. The predominance of studies based on this stainless steel is mainly due to its use for PIM and probably because of the small particle size available on the market. However, and to a lesser extent, some work is related to hot embossing of pure aluminium, copper and WC-based powders [8].

On the other hand, the binder is an element that must not exist in the final component. Analogously to μ-PIM, the binder consists of a combination of multiple organic compounds. In general, a binder system should have the following characteristics: low viscosity at the moulding temperature to fill all the mould cavities; low contact angle to be able to wet the particles thoroughly; not react chemically with the powder particles; provide strength and structural integrity to the green body to allow its handling before debinding and sintering, and it must not leave an ash trace upon its removal [12].

They generally have at least two components: a filler and backbone phases. In several cases, they also contain additives such as surface-active agents (e.g. stearates, phosphate, titanates). The filler possesses low viscosity, has a low melting temperature, and is removed in the first phase of debinding. Some typical constituents are waxes (paraffin, carnauba, polyethylene, bees), polyacetal and others. The backbone phase has a higher degradation temperature than the filler and is stiffer to provide such structural integrity to the green compact. Typical constituents are thermoplastic polymers such as polyethylene, polystyrene, polymethyl methacrylate, polyvinyl alcohol, etc. [12]. The following table (Table 1) contains examples of the characteristics of powders and binders used for hot embossing:

Table 1: Powder with the respective binders studied for hot embossing. PP, PW, and SA are polypropylene, paraffin wax and stearic acid, respectively. Adapted from [8].

Powder	D_{50} (µm)	Shape	Binder
Pure Al	10	Irregular	Commercial binder M1
Cu	6.3	Irregular	PP+PW+SA
Fe	2,5,10	-	-
Fe-8%Ni	4.4	Irregular	PP+PW+SA
SS 316L	2.0	-	Semicrystalline polymers, wax, and surfactant
	3.0	-	-
	3.5	Spherical	Commercial M1
	3.6	Spherical	Commercial Lincomont and M1
	5.0	Spherical	PP+PW+SA
	7.0	Spherical	Commercial Licomont
	D_{90}<22	-	PW based on pore-filler polymer
SS 316L (+ MWCNT)	3.5	Spherical	Commercial M1
WC-Co	0.5	-	-
	5.7	Spherical	PP+PW+SA
	6.1	Spherical	PP+PW+SA

Commercial binders do not have their composition disclosed, but they likely have at least one backbone component and one filler. The binders used in research revolve around the triad polypropylene (PP), paraffin wax (PW) and stearic acid (SA). PP acts as the backbone, and the PW and the SA carry the role of filler and surfactant agent, respectively [13].

Mixing occurs at a temperature high enough for the binder to melt. The mixing temperature should be lower than the degradation temperatures of its components. These temperatures are determined based on differential scanning calorimetry (DSC) analysis [14]. For example, for in-house binders (PP+PW+SA), PP has the highest melting temperature (around 160 ºC), so the mixing temperature is around these values [15]. That is why several studies have opted for temperatures between 150 and 180 ºC [8].

There is an effortless way to mix and assess the mixing behaviour, like torque rheometer equipment. This device registers the mixing torque over a certain period. In the beginning, there is a sudden increment in torque with adding the powder to the molten binder. Throughout mixing, the torque decreases steadily and stabilises. The stabilisation of the torque indicates that the mixture is homogeneous. Several factors modify the behaviour of the feedstock/mixture. One of them is the powder-to-binder ratio [12].

The powder-to-binder volume ratio is called powder loading or solid loading (PL/SL). Correct mixing and dosing of the binder are of paramount importance as excessive amounts severely limit the contact of powder particles (Figure 4). The oversupplied binder can lead to excessive shrinkage, heterogeneities and porosities in the part or, in extreme cases, a

complete structural collapse. In addition to that, a powder mixture underloaded with a binder is undesirable as the part can crumble during demoulding [13].

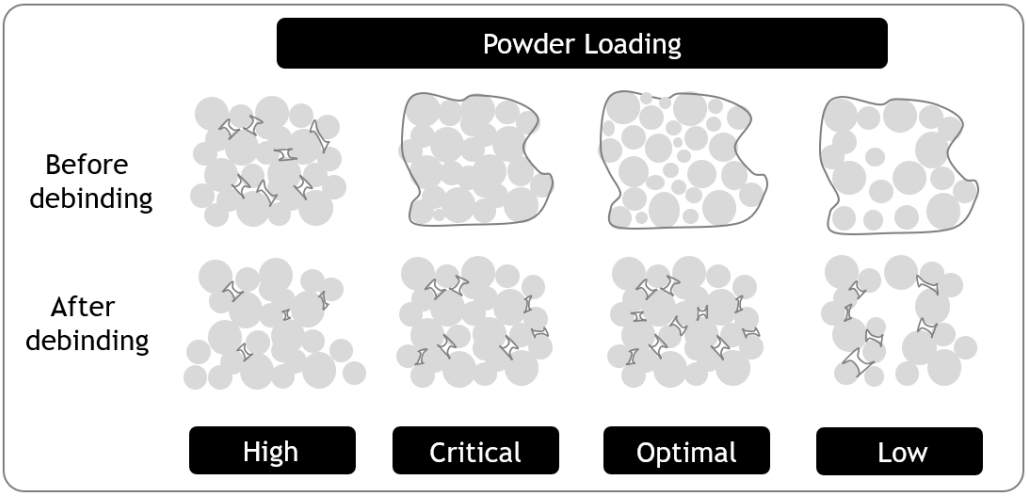

Figure 4: Illustration of the influence of different powder loading in a component.

The ideal powder loading contains enough binder to fill all the voids between the particles and simultaneously allows the powder particles to slide into the mould filling. In the borderline scenario, the binder barely covers the tightly packed particles. This volume limit is called critical solid loading (CSL) and theoretically means that the viscosity of the powder-binder mixture tends towards infinity [12].

Zhang *et al.* [14,16] studied the production of stainless steel (316L) die mould by hot embossing. In two different papers [14,16], the authors characterised the behaviour of the mixture (SS316L + in-house binder) for distinct conditions (Table 2).

Table 2: Selected conditions to test the torque mixing of a feedstock. The non-constant parameters are highlighted in bold. Adapted from [14,16].

Plot	Powder Loading (%)	Mixing rotation (rpm)	Temperature (ºC)	Binder composition (PP:PW:SA)
A	**58, 60, 62, 64, 66**	(50) constant	(170) constant	(40:55:5) constant
B	(60) constant	**10, 30, 50, 70, 90**	(180) constant	(25:70:5) constant
C	(60) constant	(50) constant	**170, 180, 190**	(25:70:5) constant
D	(60) constant	(50) constant	(180) constant	**25:70:5 50:45:5 75:20:5**

The results obtained by the authors are available in Figure 5. The results are elucidative concerning the role of the different parameters in the mixing torque values. Overall, it seems appropriate to assert the following conclusions: the mixing torques stabilised in a relatively short time frame (less than 30 minutes); the mixing torque (proportional to viscosity) raised with increasing powder loading, rotation speed, polypropylene (PP) content, and decreasing temperature.

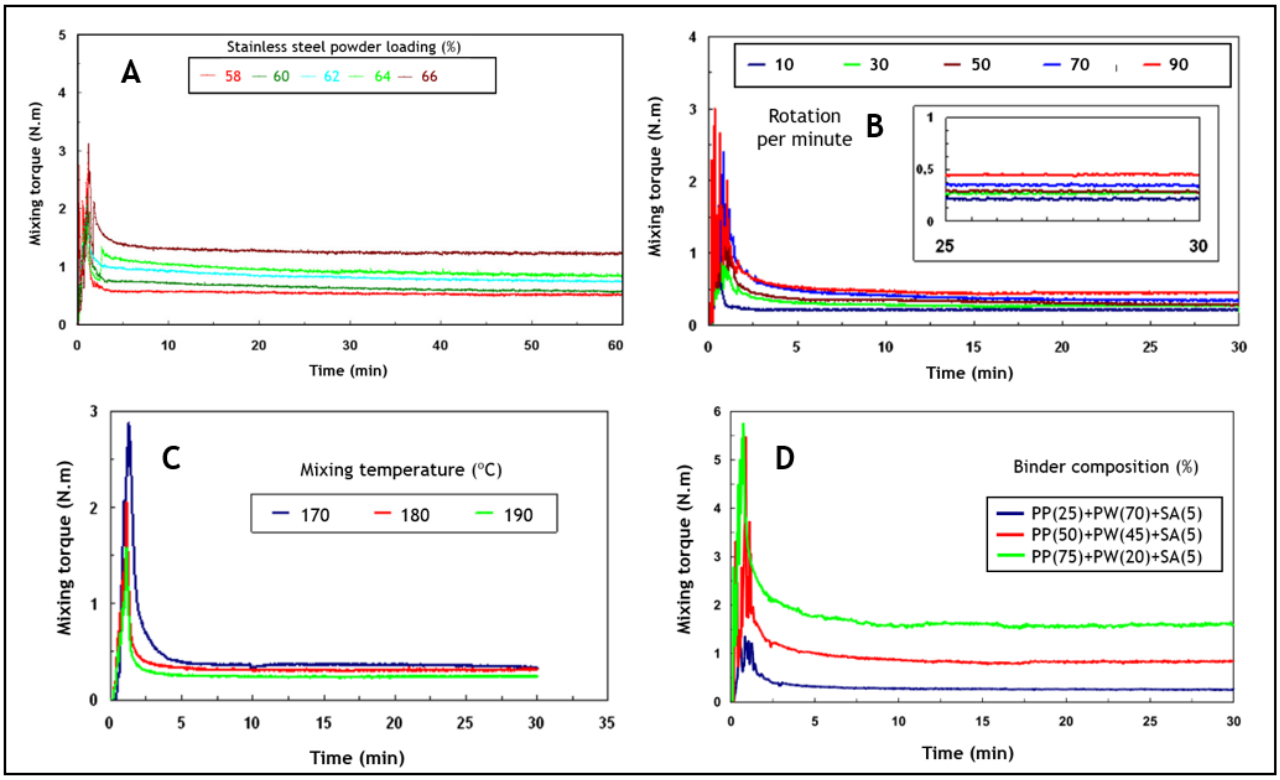

Figure 5: Effect of different parameters in the mixing torque [14,16].

These results corroborate and validate what was observed in the previous work by Sahli *et al.* [17], even when the researchers replaced SS 316L powders with copper powders [18].

One question that arises is: How to determine the optimal powder loading? To answer this, we need to figure out the critical solid (powder) loading - CSL or CSPL. The CSL corresponds to the powder loading value above which the mixing torque exhibits an erratic and unstable behaviour (inhomogeneous mixing). In other words, there will be moments in which there is a mixture of powder-binder and others where there is only a mixture of a loose powder. Therefore, one should avoid working with powder loading values very close to the critical solid loading [12].

The CSL value relies on several factors, such as the powder used and the composition of the binder. In the case of powders, for instance, Sahli *et al.* [7] studied the gradual addition of three different powders (Co-WC, Fe-8Ni, SS 316L) to a PP:PW:SA binder and found that the CSL for each mixture was 46, 62 and 66 % respectively. The authors attributed the low CSL of the Co-WC powders to their high density and coarse particle size distribution.

On the other hand, Zhang *et al.* [14] studied the gradual addition of SS 316L powders to three binders with increasing PP contents (25, 50, 75%) and observed a decrease in the CSL values (72, 68, 64 %). The CSL cutback is not perplexing since there is an increase in the content of the most viscous binder component (PP).

2.1.2. Shaping by hot embossing

Influenced by polymer hot embossing, the hot embossing of powder-binder feedstocks is also a thermomechanical process.

As previously described, the powder-binder process encompasses four elementary steps that can be distinguished: (1) heating of the feedstock and mould to the moulding temperature; (2) application of a constant pressure maintaining the temperature for a certain period; (3) cooling of the system without relieving the pressure; (4) demoulding of the green component [5].The success of replicability of a component correlates primarily with the parameters of the embossing process, namely the pressure, working temperature and holding time [8]. The holding time should be long enough for the mixture to flow into the mould cavity and allow its respective cooling, and it should also be short to reduce the processing time [19]. Concomitantly, the use of higher temperatures and pressures helps to fill all the mould cavities. Conversely, low embossing pressures and temperatures culminate in a porous and mediocre replication [20]. For example, when Sahli *et al.* [18] replicated microfluidic mould inserts with a Cu+Binder (PP+PW+SA) feedstock, they observed a higher filling ratio and a lower roughness when increasing the process temperature. However, there should be a maximum ceiling imposed on those parameters because when the temperature is disproportionally high, there is a premature degradation of the binder responsible for the integrity of the green body. To this end, and once more, the data provided by the DSC analysis enters the picture [13].

In turn, the high pressure when compressing the green part against the mould compromises the easy demoulding of the component and causes excessive thinning of the embossed substrate [21].

Regarding demoulding, some works, such as those of Fu *et al.* [21] and Sequeiros *et al.* [22], have adopted silicone moulds to facilitate demoulding. Although the researchers have successfully produced and demoulded some parts, they have noticed some problems. In the case of Fu *et al.*'s work [21], the issues arose from the high aspect ratio of the microstructures. A high aspect ratio can result in cracking and imprisonment of microstructures in the mould (Figure 6A).On the other hand, in Sequeiros *et al.* [22] work, they studied the influence of different pressures (4, 7, 14 and 28 MPa) in the embossing of 316L stainless steel parts. Their problems arose from the high pressure applied to some samples. The high pressure can distort the silicone mould and the geometry of the green part. Although the authors used silicone moulds and releasing agents, the parts still broke apart during demoulding (Figure 6B).

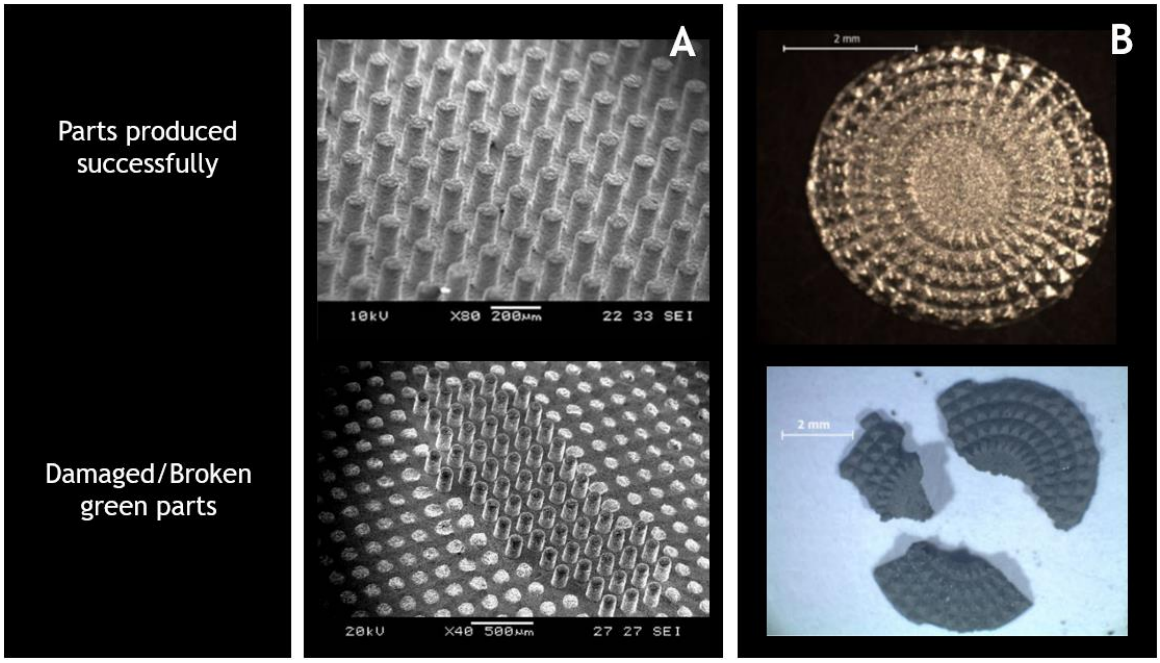

Figure 6: Successfully produced and broken parts from A) Fu and B) Sequeiros. Adapted from [21,22].

The definition of the best conditions to perform hot embossing is an iterative process of trial, error and improvement. Unfortunately, like any other manufacturing process, the change of geometries and materials implies adjustments in the defined parameters, particularly those of the embossing stage.

2.1.3. Debinding and sintering

After the successful demoulding of the green components, it follows a debinding and a sintering stage.

In the debinding stage, the binder should be removed almost in its totality in the shortest possible time, without impacting the moulded parts, i.e., with a good surface finish and reduced porosity. There are two ways to perform the green body debinding: solvents or thermal cycles [13].

In the case of solvent debinding, it is more applied to dissolve the binder's filler (typically a wax). Therefore, it is necessary to complement the debinding with a thermal cycle to reduce the backbone content in the remaining binder [13]. For instance, Cahill *et al.* [23] subjected hot-embossed microneedles with pore fillers to a debinding in ethanol and subsequent isothermal stages to eliminate the remaining binder and pore fillers. The presence of pore fillers was intentional since the author's purpose is to target microneedles for drug delivery.

In a comprehensive review by Sequeiros *et al.*[8], it is noticeable that most studies embrace the thermal debinding approach. Thermal debinding comprises two stages - primary and secondary debinding [13]. In primary debinding filler degradation take place and the formation of an interconnected network of pores. Removing this primary binder is slow to avoid the cracking and distortion of the component. The duration of the primary debinding is proportional to the size of the part to produce, which means that it is a time-consuming step for a sizable component. Although most metal injection moulding (MIM) processors have discontinued this primary stage, it is still advantageous for powder hot embossing [13].

In secondary debinding occurs the elimination of the backbone by degradation. This secondary binder escapes more easily from the component because of the interconnected pore network created by the primary debinding. After the thermal cycles, the outcome is a very fragile part with residual binder contents called the brown part [13].

The definition of the thermal cycles, namely the temperatures to be imposed, are determined with thermogravimetric analysis (TGA) [8,13,22]. For the in-house binders (PP+PW+SA), some of the published works [4,7,14,16,18,19] adopted cycles with two specific temperatures. The explanation for these temperatures lies in the temperatures for the complete degradation of the PW/SA (filler/additive) and the PP (backbone) duo. According to the experimental data, the overall degradation of PW/SA and PP ends at around 330 and 450 ºC, respectively. Based on these results, it seems to be a consensual practice that the debinding consists of a 350 ºC stage (PW/SA elimination) followed by a 500 ºC stage (PP and residual binder depletion).Regarding the duration of the stages, most authors [4,7,14,16,19] employ 30 minutes for each isothermal step, and others use 60 minutes [18]. In the case of commercial binders such as *Lincomont* or commercial M1, some existing publications impose quite long times (4 to 5 hours for each stage) [22,24]. Despite the differences in the extent of the debinding times, the general observation of the authors is that there are no significant dimensional changes.

The phase following the debinding is sintering. Sintering is a thermal process in which the brown component composed of an aggregate of separate powder particles consolidates. The consolidation provides compulsory strength in the finished product [13,25].The process takes place at high temperatures but below the melting temperature of the metal. In many cases, metals are susceptible to oxidation at elevated temperatures. For this reason, the sintering step occurs in a controlled atmosphere and vacuum furnaces [13,25]. Other parameters to control during the procedure are the sintering temperature, heating rate, sintering time, and cooling rate. It is perceived in the studies [14,19] that the elevation of the sintering temperature helps the densification of a compact. In turn, denser components present a better mechanical performance [14,19]. However, according to the works of Sahli *et al.* [18], one should pay attention to the temperature applied to avoid loss of geometric details since excessively high temperatures end up rounding the edges. High heating rates are beneficial in the sense that they reduce the possibility of grain size growth. In other words, a lower heating rate means a lengthened stay of the compact at temperatures below that of sintering, i.e. it prolongs the duration of the thermal cycle [26].

A liquid phase (the melting of one of the components) during sintering, like in WC-Co powders, usually assists in the diffusion processes, reduction of pore size, increasing density and improvement of hardness [27]. Unfortunately, its presence is not always desirable. For example, in a study by Sahli *et al.* [7], when the authors try to replicate microchannels in microfluidic devices with WC-Co powders, they state that the presence of a liquid phase interferes and substantially distorts the geometry of the microcavities. For this reason, they decided to sinter the parts at a temperature below that of a liquid phase formation. It is safe to say that a liquid phase acts as a "double-edged sword" in sintering.

The sintered components are then assessed according to various parameters. These mainly relate to their final application.

In applications where the final surface quality matters, some factors such as detail replication, surface roughness and surface defects are critical. For example, we could cite the engraving of details on microfluidic devices for the biochemical sector. These devices are microreactors (size of an electronic chip) with narrow channels where complex chemical analyses are performed. It means that a poor replication of details and high roughness leads to poor circulation or transport of fluids through specific paths [16,18,28]. Another example is micro inserts for manufacturing optical components such as LED lenses. Poor replication or excessive roughness of the inserts would seemingly result in lenses with different optical properties than the intended ones [8].

In addition to surface quality, evaluating the porosity and mechanical behaviour of the sintered components are relevant. Some parts, such as mould inserts, should have the sufficient mechanical strength to withstand the mechanical stress imposed on the mould. The mechanical behaviour and porosity are directly related to the processing conditions. For example, in the work of Sahli *et al.* [19], the authors recorded a drastic increase in the density of WC-Co parts from 73% to 97.8% when they increased the sintering temperature from 1300 to 1350 ºC. The hardness of the components also improved significantly with an increment of almost 20 HRA.

Although there are differences in the materials used, other authors, such as Zhang *et al.* [16], also recorded congruent results for 316L steel. By reducing the porosity from 4 to 2%, the hardness increased significantly from 187 to 198 HV.

However, maximising the mechanical properties and density may not always be fundamental. In the biomedical field, although a network of interconnected pores compromises the mechanical properties of components such as hot embossed microneedles, their presence is beneficial for storing dry medicines, followed by their controlled release on skin contact [23].

2.2. Additive manufacturing (AM)

It is well-known that AM techniques cannot compete with the mirror-like surface finishing and accuracy given by conventional material removal processes. But the geometrical freedom, minimal material waste, and reasonable cleanliness make these technologies enticing [29].

Several technologies regarding AM of metals are available in the market. Most of these processes use a laser as an energy source. These technologies are powder feeding (PF) and powder bed fusion (PBF) systems [30,31].

Technologies based on powder feeding systems assume several designations, such as directed energy deposition (DED), direct metal deposition (DMD), powder blown additive manufacturing, or canonically laser cladding. For simplicity purposes, we will call it DED.

The operation of DED, briefly, consists of the output of a laser beam through a nozzle that will irradiate the substrate surface. The irradiation partially melts the substrate and forms a melt pool. Simultaneously, a material, usually a powder, is injected and will absorb some of the laser energy. The preheated powder will melt in contact with the melt pool. The synchronised movement of the laser and powder feeder leaves in its path a cladding layer [32,33].

It is possible to highlight laser powder bed fusion (LPBF) and electron beam melting (EBM) within the powder bed fusion technologies. A concise description of the two technologies would be that the two techniques depend on the selective melting of the desired portion in a powder layer under vacuum conditions. The vertical construction of the component is ensured by a repetitive cycle of replenishment with a new powder layer and melting portions of the new layer. The main difference between LPBF and EBM is the energy source: laser for LPBF and electrons for EBM [34,35].

The following Table 3 compiles some examples of work where AM is applied in the production of inserts:

Table 3: Some examples of mould inserts produced with different additive manufacturing technologies.

Technology	Materials	Application	Observations	Ref.
Laser powder bed fusion	Maraging Steel	High Pressure Die Casting Die Inserts	The as-built surface roughness was around 12 µm. Extensive machining was needed to reach the required tolerance and surface finishing. The inserts were age hardened to 53 HRC.	[36]
Laser powder bed fusion	Maraging Steel	Mould inserts with mirror-like surfaces	The mirror-like surface is obtained with the help of electroforming. The density was under 99.5%.	[29]
Selective laser sintering	Maraging Steel	Tool insert for the automotive industry	Roughness after polishing of 0,07 ± 0,01 µm. Hardness of 38 HRC (as-built).	[37]
Direct metal deposition	Nimonic 80A	Die inserts for liquid forging	Both powder feed rate and z-increment significantly influenced the lack of fusion and porosity. Porosity above 0.01%. Hardness between 257–275 HV.	[38]
Laser powder bed fusion	H13 tool steel	Tool Steel Die Insert for Pressure Die Casting	Porosity of 0.13%, the surface roughness values ranged between 1.8 and 3.5 µm. UTS of 1895 MPa and YS of 1550 MPa and measured elongation of 10% (as built).	[39]
Laser powder bed fusion	H13 tool steel	Insert for extrusion dies	Hardness of 48 ± 2 HRC (as built). No melt pool boundary segregations were visible after heat treatment.	[40]
Electron beam melting	H13 tool steel	Injection moulding tool inserts	There was no significant difference in machinability between EBM produced H13 insert and the inserts manufactured from the H13 steel plate. EBM process has limitations regarding small features.	[41]

In contrast to the more outspread beam-based approaches, binder-based technologies do not rely on melting and solidification as bonding mechanisms between particles. The particle bonding occurs during sintering by diffusion [42].

For example, polymeric binder systems are binder jetting and material extrusion (ME). In this chapter, it seems appropriate to shift the focus from hot embossing to technology with similar green part post-processing: binder jetting and ME (also called fused filament fabrication).

In binder jetting, layer-by-layer construction is ensured by dropping a binder in the desired portions of a powder bed. Similar to LPBF/EBM, the vertical construction of the component consists of a repetitive cycle of replenishment with a new powder layer and deposition of binder in specific portions of the new layer. The binder removal and densification of the obtained component occur in a debinding and sintering stage.

In ME, the layer-by-layer building is accomplished with a feedstock. In contrast to hot embossing, the ME's feedstock has to be in the form of a filament. Then, the filament enters

an extrusion system. The extrusion ensues through a nozzle that will soften the binder in the filament and allow its deposition. After printing, the green part suffers debinding and sintering steps (Figure 7) [43].

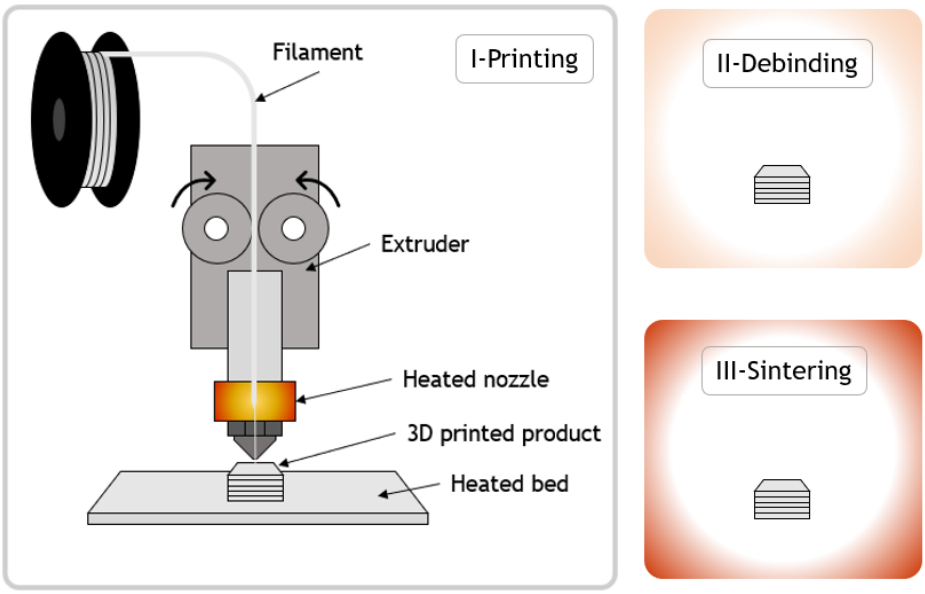

Figure 7: Scheme of the material extrusion processing and post-processing. Adapted from [43].

Although the reports about ME technology as a possible AM method appeared in the 1990s (focus on polymeric materials), the detailed reviews on the process for metal powders just appeared later. One such study is that of Wu *et al.* [44]. In this paper, the authors described the main aspects of a ME process, like the preparation of feedstocks, the optimisation of layer-by-layer deposition process parameters and brief descriptions of subsequent debinding and sintering steps. Roughly speaking, ME is a process similar to hot embossing in several ways, with the main difference in how the feedstock gets shaped into the desired geometry.

Like any other manufacturing process, ME also has relevant process parameters. The printing process has several input variables, like extrusion temperature, build plate temperature, printing speed, layer thickness, extrusion width, toolpath and slicing strategy [45]. Besides these parameters, we should not forget the parameters associated with the post-printing steps, like the debinding and sintering cycles. So, it is crucial to define them correctly to produce acceptable components.

But unfortunately, in the AM industry, it is uncommon for manufacturers to make available devices with disclosed and open-source parameter settings. Therefore, it is frequent to adopt iterative printing methods to define processing windows [46].

Nonetheless, the mechanical properties of the products obtained can be comparable to those obtained by conventional methodologies. For example, Costa *et al.* [47] produced several components by ME to evaluate them and compare their mechanical properties with the manufacturer's reference values (Figure 8). The author used three distinct alloys: Inconel 625, H13 SAE, and 17-4PH.

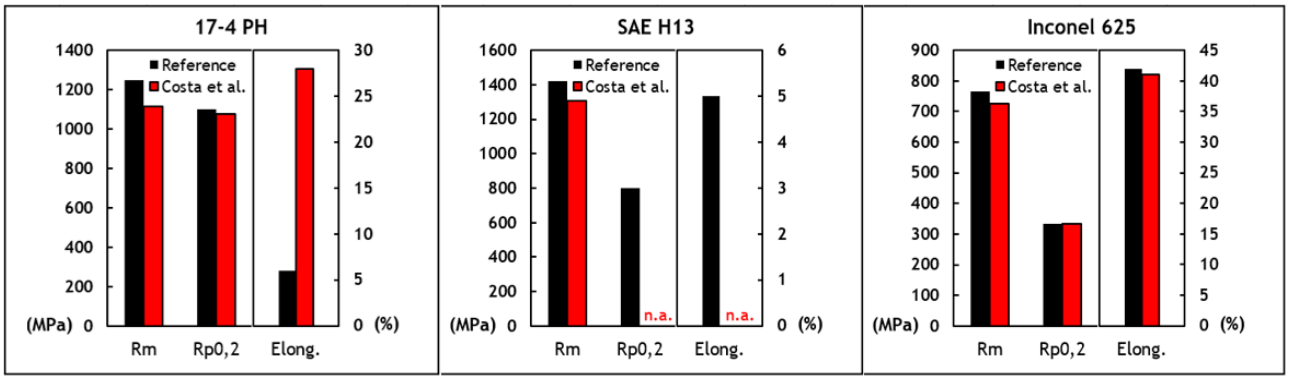

Figure 8: Comparison of mechanical properties from three distinct materials. Adapted from [47].

Although the authors encountered problems in the mechanical testing of the SAE H13 alloy and anomalous elongations for the 17-4 PH alloy, the remaining results in the experimental work are not very dissonant with the intended reference values.

After the brief description of the various AM processes, we consider it pertinent to leave here some miscellaneous regarding the advantages and disadvantages of these technologies:

Table 4: Some advantages and disadvantages of different AM technologies. Adapted from [48]

Technology	Advantages	Disadvantages
Directed energy deposition	Relatively fast material deposition; Dense parts with high mechanical strength;	Low build resolution; Poor surface quality; Less geometrical freedom; Expensive machines
Laser powder bed fusion	Very complex shapes like thin walls, hidden holes, and porous structures; Good mechanical properties of the final part; Decent surface quality	High cost; Corrosion sensitive; Need of post heat treatment; It requires to build structures for more extensive and heavier metallic parts.
Electron beam melting	Better contamination protection; Parts with low levels of residual stress; Minimal need for supports	Possibility of electrostatic charging the powder
Binder Jetting	No need for construction supports; Fast process; Suited for a wide range of materials; Suitable for large components	Limited success for metallic parts; Lower density and worse mechanical properties compared to those obtained in PBF processes; Post-processing (debinding and sintering)
Material extrusion	Simple technology; Wide range of materials; Low-cost machines available (for polymers)	Low accuracy; Nozzle wall under shear stress; Post-processing (debinding and sintering) and inherent shrinkage

3. Experimental Procedure

3.1. Task planning

Before concretely describing the experimental materials and methods, it seems pertinent to provide an outlined description of the planning of the work to be carried out hereafter.

First and foremost, to execute a comparison between the hot embossing and fused filament fabrication, this work emphasises feedstocks of an in-house blend (SAE H13:M1) for hot embossing and a wired filament (SAE H13: unknown binder) for ME.

The production of components with the in-house mixture starts with the binder characterisation using thermal tests to determine the most suitable working temperatures. Then, it proceeded with a mixture optimisation to define the best powder to binder ratio to perform the hot embossing.

The conditions to perform the hot embossing, debinding and sintering of the optimal mixture of SAE H13:M1 will be based on the work of Sequeiros *et al.* [20].

As for the ME, the filament is directly employed in producing components without any previous optimisation.

ME filament was used to perform the hot embossing. For that, and similarly to the in-house mixtures, there was a thermal characterisation of the filament (pure binder unavailable for testing) to define the working temperatures. Afterwards, the filament was ground and submitted to hot embossing. Unfortunately, there are no studies regarding the embossing of this filament. So the parameters for its execution were undertaken with a design of experiments. The following Figure 9 illustrates the various stages involved in this study.

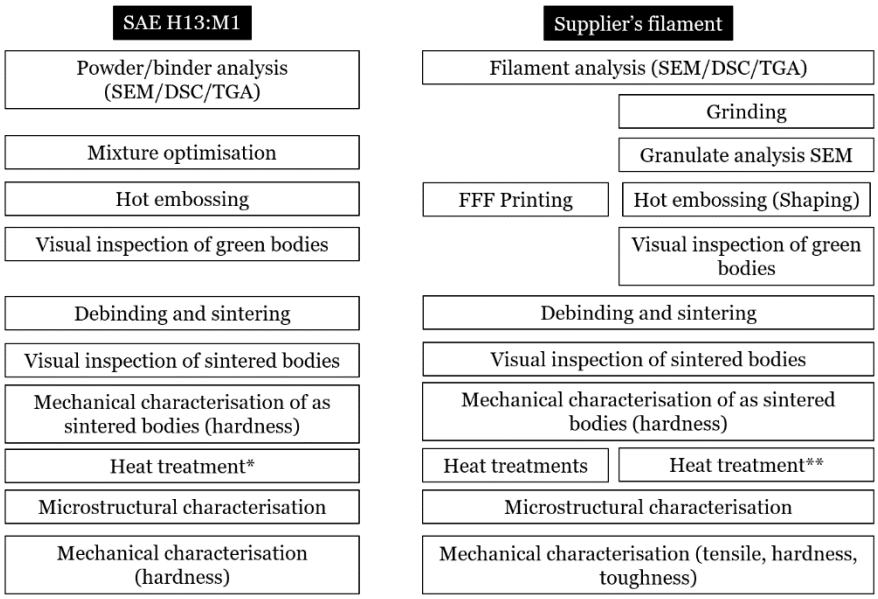

Figure 9: Overview of the experimental procedure.

3.2. Target geometry

The desired geometry corresponds to a semi-sphere with pyramidal details to produce lenses for automotive vehicles. Although we do not have the technical drawing of the final component, the original metallic mould to produce the geometry is shown in Figure 10A. The necessity to produce the component by AM for the intended comparison lead us to recreate the design by computer aided design (CAD) software. The CAD design (Figure 10B), conceived in *Fusion360* (Autodesk) software, tried to get as close as possible to the geometry of the insert.

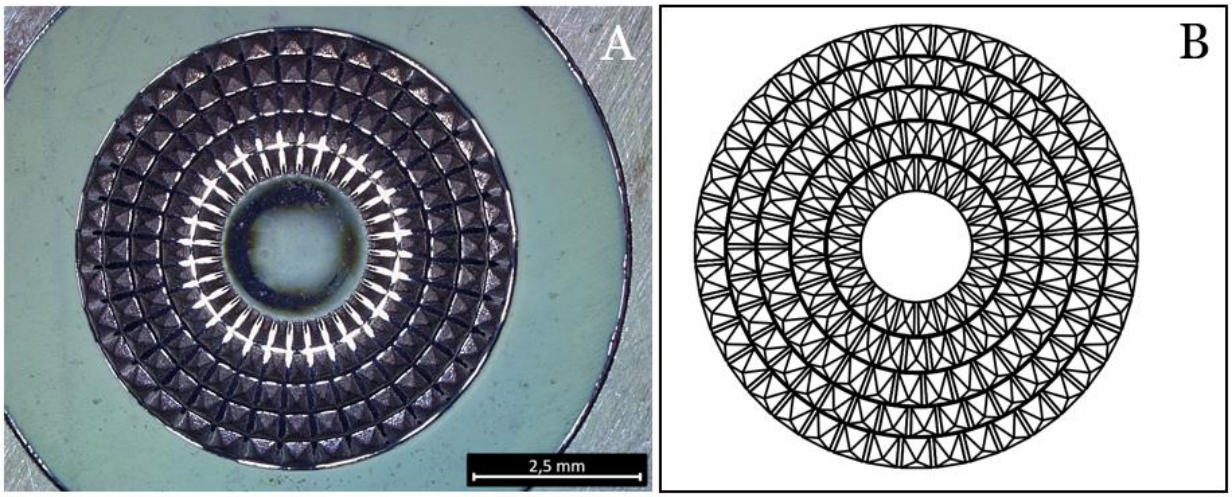

Figure 10: A) Metallic model produced by EDM and B) CAD recreation of the model geometry.

3.3. Materials

The materials used to produce the SAE H13:M1 mixture were metallic powders of SAE H13 tool steel and a commercial binder designated M1 and provided by *Atect*. The SAE H13 is an air-hardenable, hot work tool steel suitable for injection moulds [49]. The M1 is a suitable binder for PIM and has a base composition of a mixture of polyolefin waxes and polyethylene. Furthermore, it was used a silicone rubber die (38 ± 1 Shore A Hardness) to replicate the desired geometry by hot embossing (Figure 11). The silicone rubber die was obtained from the metallic mould.

The analysis of the SAE H13 metal powders was carried out by using the following techniques: laser diffraction in a *Mastersizer 2000* (Malvern) analyser for particle size analysis and Scanning Electron Microscopy (SEM) in a *Quanta 400FEG* (FEI) microscope for particle morphology.

Before mixing, the binder got assessed by a DSC and Thermal Gravimetric (TG) analysis. These tests make it possible to evaluate the mass variation and the phase transformations that occur in the binder at high temperatures. For this purpose, the tests were performed in a *Setsys* (Setaram) calorimeter under an argon atmosphere and with the following settings: heating rate of 10 ºC/min from room temperature up to 700 ºC.

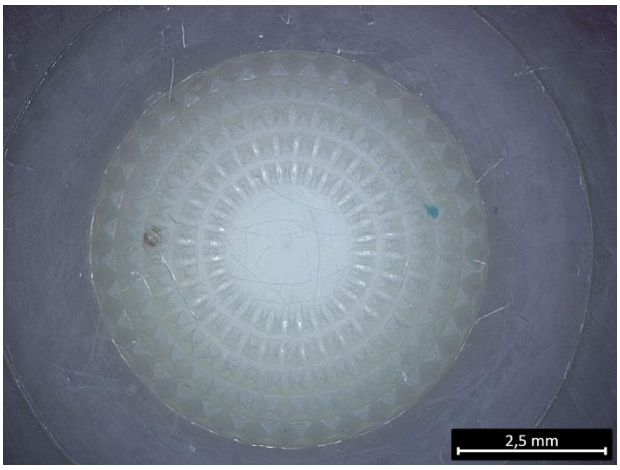

Figure 11: Transparent silicone rubber mould after use.

For the ME, the material in question is a wired feedstock (d=1.75 mm) supplied by *Markforged*. The feedstock comprises the same type of tool steel (SAE H13), with the difference being its binder composition, which is unknown. In the following table is the typical chemical composition of SAE H13 steel:

Table 5: Chemical composition of the SAE H13 tool steel [50].

Element	Cr	Mo	Si	V	C	Mn	P	S	Fe
wt%	4.7-5.5	1.3-1.7	0.8-1.2	0.8-1.2	0.3-0.45	0.2-0.5	<0.03	<0.03	Bal.

For hot embossing of the filament/wired feedstock, the material is a fine granulate obtained by grinding the same *Markforged* filament in a coffee grinder. A more detailed description of the tested methods for grinding the filament can be found in Appendix I (Figure 43).

3.4. Feedstocks characterisation and optimisation (SAE H13:M1)

Through the analysis of the data previously obtained, the next step consists in defining the best powder-binder ratio (SAE H13:M1) that allows the successful execution of all subsequent stages of hot embossing. For this work, different powder-to-binder ratios were tested: 60:40, 57:43 and 55:45. The evaluation was carried out in a *Brabender Plastograph* rheometer, and the methodology consisted in adding the powder to the binder in the viscous state. The rotor blade speed and the mixing temperatures were 30 rpm and 160 ºC, respectively. The selection and definition of the ideal powder-to-binder ratio are achieved through the evaluation of the rheological behaviour of the mixture, i.e., the torque variation over time.

After obtaining the mixture with the ideal solid loading ratio, SEM images of the mixture were taken using the same microscope.

3.5. Feedstock characterisation (filament)

The powder-to-binder ratio of the filament is unspecified, and since the binder present is also unknown, it was not possible to analyse it separately from the feedstock at a thermal level. Therefore, the filament was subjected to DSC and TGA tests as it was supplied. The DSC test occurred in a *DSC 214 Polyma* (NETZSCH) under a nitrogen atmosphere. The TGA test occurred in a *STA 449 F3 Jupiter* (NETZSCH) under an oxygen and helium atmosphere. The thermal tests were carried out under the following conditions: heating rate of 10 ºC/min from room temperature up to 200/500 ºC (DSC/TG).

The filament and granules were observed in the same SEM equipment mentioned above.

3.6. Design of experiments (SAE H13:M1 and granulated filament)

The hot embossing conditions tested in this study were based on previous studies [20], where the same binder and configurations were used. Binder has a primordial effect on critical hot embossing parameters, but the powder characteristics also influence the feedstock viscosity behaviour. The conditions tested are present in Table 6.

Table 6: Conditions tested for SAE H13:M1 feedstock.

Temperature (ºC)	Pressure (MPa)	Holding time (min.)
210	8.00	30
220	5.33	30
220	8.00	30
220	8.00	45
230	8.00	30

Regarding the hot embossing of the granulated filament, it was set up a design of experiments (DOE) (Table 7) to evaluate the effect of the embossing parameters on the detail's replication. The temperature, pressure and embossing time are in the following ranges: [190-210 ºC], [5.33-8 MPa], and [30-45 minutes], respectively. The heating and cooling rates were constant at 15 ºC/min. For each condition, it was produced three parts.

Table 7: Design of experiments for hot embossing of the filament.

Temperature (°C)	Pressure (MPa)	Holding time (min.)
190	5.33	30
	8.00	30
	5.33	45
	8.00	45
200	5.33	30
	8.00	30
	5.33	45
	8.00	45
210	5.33	30
	8.00	30
	5.33	45
	8.00	45

3.7. Mixture shaping

The granulated mixture was carefully poured into the silicone rubber die and covered with a silicone cover. Before the embossing step, the walls of the metallic matrix and the metallic support disc were sprayed with a silicone-free mould release agent. The silicone die assembly is then placed into the metal matrix and subjected to the forming stage. To perform the shaping stage of hot embossing, we used the following types of equipment: a *LLOYD* Instruments LR 30K mechanical testing machine in compression mode and an infrared radiation furnace.

The metallic matrix was placed on top of the lower molybdenum punch. Then, the top molybdenum punch was lowered until it touched the red silicon cover. After that, the furnace was mounted around the assembly, and compression and heating began. Figure 12 shows a schematic of the configuration of the described system. The mechanical testing machine controlled the embossing pressure. The temperature and the processing time were managed by the controller of the furnace programmed with the intended thermal cycle.

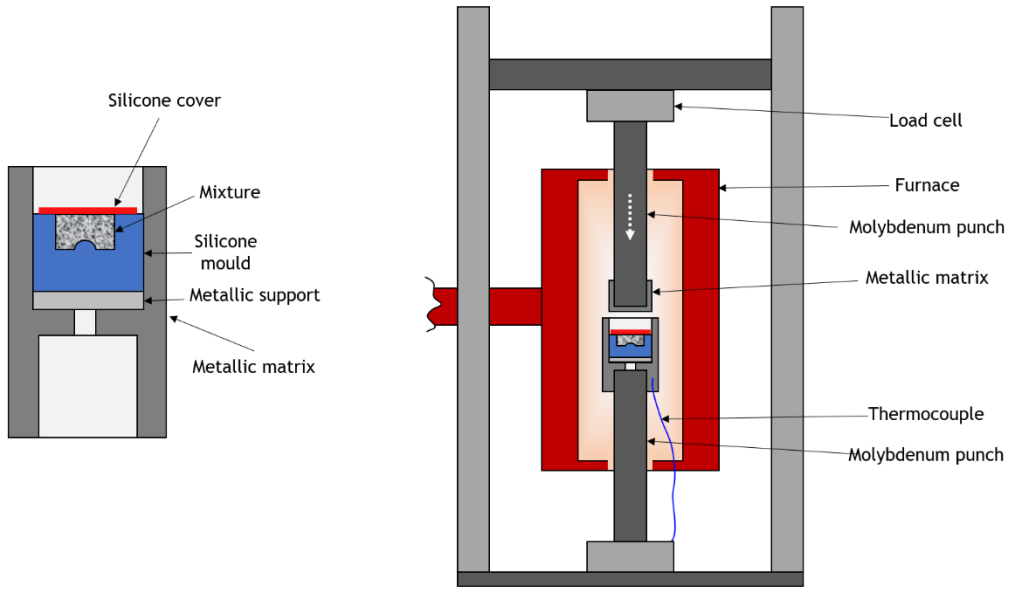

Figure 12: Assembly of the silicone mould inside the metallic matrix (left) and its positioning in the mechanical testing machine (right).

3.8. Samples production by material extrusion

Besides the target geometry, the following parts for the mechanical tests were designed in the *Fusion360* software (Autodesk): five cubes (l=10 mm) for further heat treatments and six tensile specimens. The technical drawing of these samples can be seen in Figure 13. Then, the slicing step occurred in the *Ultimaker Cura* software with the following parameters: 100 % infill, 0.20 mm layer height, 0.40 mm deposition line width, and no additional construction supports. The component was printed in a *Metal X* printer (Markforged). The parameter settings are XYZ orientation of 90º, 0º, and 180 º, and a post-sintered layer height of 0.125 mm.

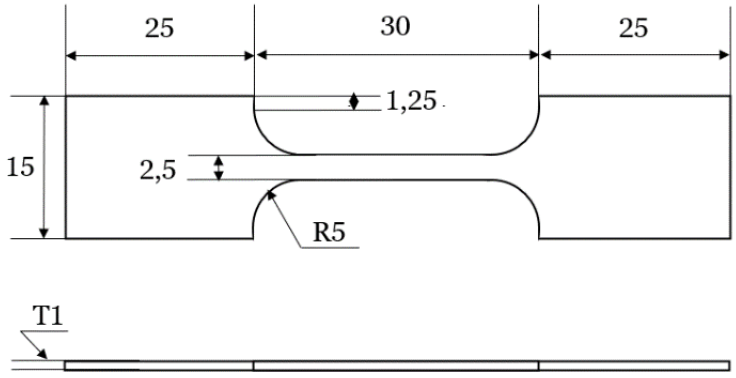

Figure 13: Technical drawings of the tensile specimen (units in mm).

3.9. Debinding and sintering

The debinding and the sintering of the SAE H13:M1 parts followed the thermal cycles illustrated in Figure 14. The sintering cycle was based on previous studies and bibliography [8,20,22,51] and TG/DSC results. Both thermal processes were performed in a high-temperature furnace coupled with a vacuum and gas introduction system. The pressure and atmosphere employed inside the furnace were 5×10^{-2} mbar and hydrogen argon, respectively.

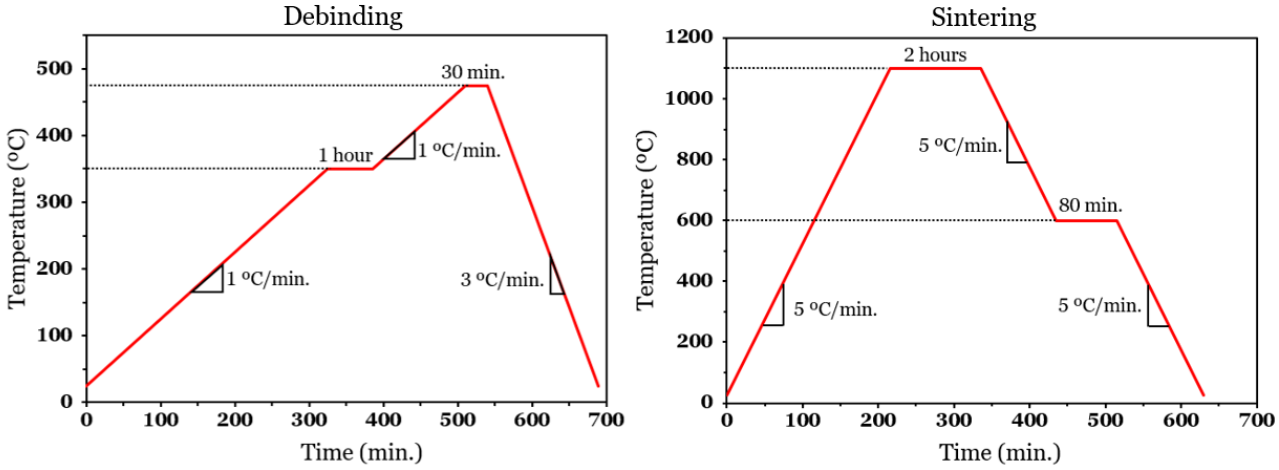

Figure 14: Debinding and sintering cycles for SAE H13:M1 parts.

As for the components produced with *Markforged* filament (by ME or hot embossing of the granulated filament), they underwent two hours of solvent debinding with a *WASH-1* (Markforged) solution to open the interconnected microchannels. The interconnected pores inside a printed part body allow the gases that formed during subsequent thermal debinding to escape. The next step is thermal debinding and sintering. Both debinding and sintering of the cubes and tensile parts were carried in a *Sinter-1* furnace (Markforged). Unfortunately, the thermal cycles are unknown to the user.

The hot embossing components and the sample with the intended geometry (produced with AM) were debinded and sintered following the cycles presented in Figure 15 and created by us. The cycles were based on DSC and TG results, and the sintering cycles were based on the different literatures [8,20,22,39,51] The thermal processes are carried out in a horizontal resistance furnace (Termolab) (different from the previous one). The pressure and atmosphere employed inside the furnace were 0 bar and hydrogen argon, respectively.

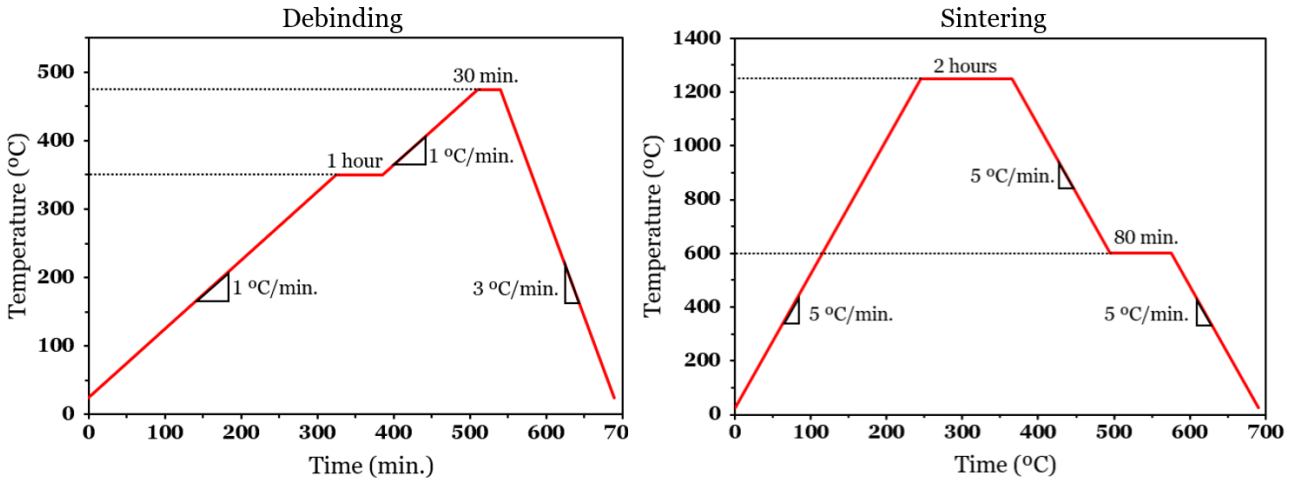

Figure 15: Debinding and sintering cycles for SAE H13: unknown binder parts.

3.10. Visual inspection and microstructural analysis

The judgement of the best hot embossing conditions depends on the quality of replication of the microdetails. Therefore, it is imperative to evaluate, visually, the produced parts.
The surface quality of all green bodies produced by hot embossing was observed and assessed under a digital microscope Leica *DVM6*. From the optical evaluation, only the unscathed components with the best detail replication advanced to the debinding and sintering steps. Then, the sintered parts were observed again under the digital microscope.
Apart from the superficial inspection, the components were prepared by conventional metallography methods for microstructural visualisation: cutting (diametrical axis), resin mounting, polishing with SiC abrasive sandpapers (180-240-400-600 mesh) and finishing with diamond suspensions (6 and 1 µm).
Microstructure observation was carried out using a Leica *DM4000M* optical microscope. The image collection was accomplished with a Leica *DFC420* camera and LAS Leica software.
As for the components produced by ME, the microstructural analysis was done on only one of the cubes. For this purpose, the cube was cut in half, polished and finished the same way as the hot embossing parts.
The hot embossing components and the ME cube were also analysed at the microstructural level after a chemical etching with an ethanol solution containing 4% nitric acid and 3% picric acid.

3.11. Mechanical characterisation

In this work, the metallic components are originated from non-conventional manufacturing processes. It is arguable whether their mechanical performance is comparable to those produced by conventional means. So, it is relevant to conduct tests regarding the mechanical properties of the parts.

The mechanical evaluation of the hot embossed components was performed only with Vickers microhardness tests since no suitable moulds were available to manufacture other kinds of test specimens. A *Duramin* (Struers) microhardness tester and Duramin 5 software was used to perform the microhardness tests. The procedure followed the ISO 6507-1 standard with a load of 0.1 kgF.

The components produced by ME followed similar mechanical tests. The etched cube was subjected to Vickers macro hardness testing in a *Duravision* (emcoTEST) durometer following the same ISO standard but with a load of 30 kgF. Microhardness tests were also employed for comparison purposes with a 0.1kgF indentation load.

The tensile tests took place in Shimadzu equipment and followed the ISO 6892-1 standard. The displacement applied was 3 mm/min.

3.12. Heat treatments

Tool steels such as SAE H13 need good mechanical strength to perform their functions. Therefore, it is usual to apply heat treatments for mechanical properties improvement.

To select an ideal thermal cycle, we performed quenching and tempering heat treatments of the cubes produced by ME. The quenching consisted of a one-hour isothermal stage at 1020 ºC followed by oil quench. Afterwards, the samples were individually tempered at different temperatures (300, 350, 400, 450, 500, 550, 600 ºC) and air-cooled. Note that for the tempering treatment, the specimens were placed on a bed of charcoal and covered with iron filings to avoid a decarburisation phenomenon.

After the heat treatments, the cubes were cut in half and metallographically prepared. Etching and microstructures observations followed the same procedure described above in 3.10.

The quenched and tempered parts were subsequently subjected to macro hardness tests with a load of 30 kgF. Based on the results, the most suitable heat treatment was selected to be applied to the best parts obtained by hot embossing.

Finally, the tensile specimens were also heat-treated, and the respective tests described in a previous topic (3.10) were employed.

4. Results and Discussion

This chapter will present the results concerning all the experimental work carried out. The structuring of the results and their discussion will adopt the following order:

- Hot embossing of the in-house mixtures (powders, binders and mixing behaviour characterisation, visual assessment of the parts)
- Material extrusion (filament characterisation, visual assessment of the parts)
- Hot embossing of the ground filament (visual assessment of the parts)
- Mechanical, microstructural characterisation, and heat treatments of the components.

4.1. Hot embossing of in-house mixtures

4.1.1. SAE H13 powders and M1 binder characterisation

Starting with the individual SAE H13 powders, we can observe from the graph in Figure 16 that the particle size distribution does not follow an utterly unimodal distribution The powder shows a clear peak around 650 µm and a second one more subtle around 200 µm. Through the cumulative curve, it is possible to identify a d_{10}, d_{50}, and d_{90} of 132, 477, and 953 µm, respectively.

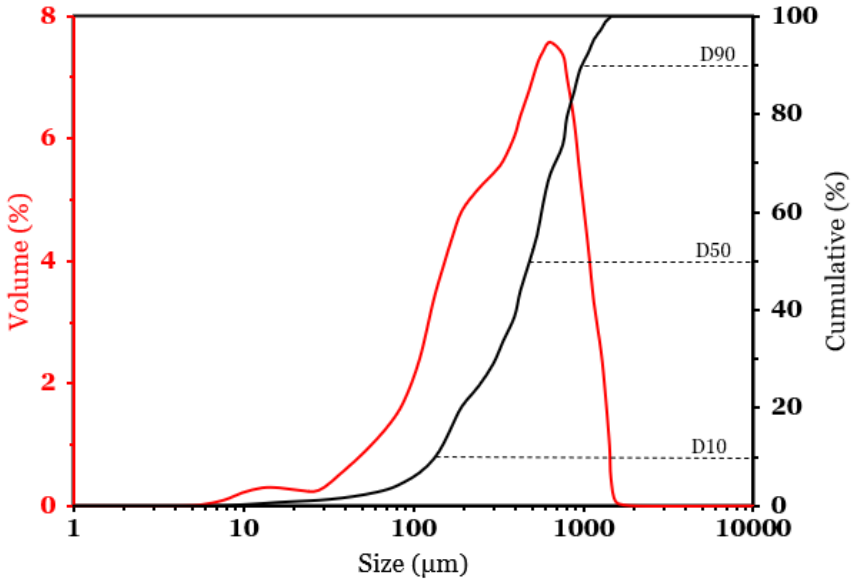

Figure 16: H13 powder size distribution.

The irregularity of the particle size is also confirmed by SEM analysis present on Figure 17. We can easily see that the morphology of the particles is partially irregular. Some particles have a spherical aspect, and others have a more elongated, rodlike, asymmetrical appearance. It is also possible to detect the presence of several smaller particles (satellites) attached to the larger particles. The existence of satellites results from the metallic bonding

between the smaller and larger particles in the semi-melt state that originated in the powder manufacturing process. However, some of these satellites may be due to particle cohesion and agglomeration phenomena. Agglomeration is primarily related to inter-particle attraction forces such as Van der Waals. The satellites and agglomeration increase the equivalent powder size and will comprise a large proportion of non-spherical particles in the powder feedstock. The irregularly shaped powder clusters hinder the filling of the inter-particle voids and the mould's intricate cavities during the feedstock shaping process [52].

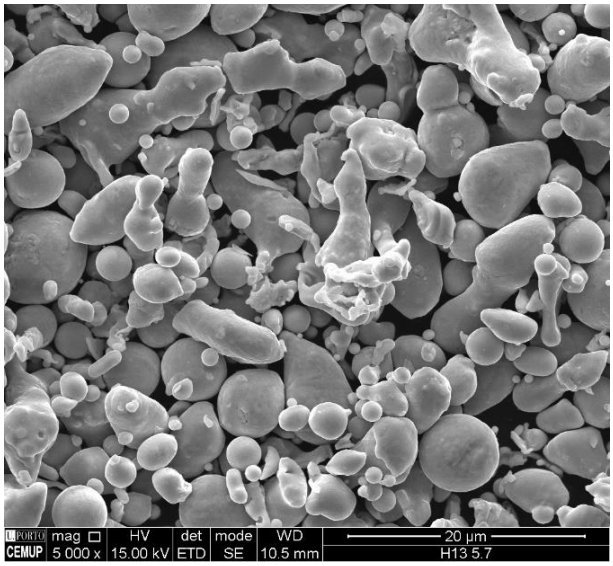

Figure 17: Scanning electron microscopy image of SAE H13 powders (secondary electrons mode).

A quick inspection of Figure 17 shows indirectly that the powders do not possess the particle size determined by the laser diffraction technique. The particles do not even appear to exceed 20 µm, which casts serious doubts regarding the earlier particle size distribution analysis. But one can easily understand the inaccuracy given that non-spherical particles, satellites, and agglomeration phenomena strongly bias the results. These factors lead the equipment to assume that there are much larger particles [53]. Therefore, it seems more plausible to accept the d_{50} value provided by the supplier (5.7 µm) as the average particle size.

The binder M1, by analysis of the DSC curve (Figure 18A), has a set of convoluted peaks. We could say that there is a range of endothermic variations situated in the interval from 50° C to 200° C. This range corresponds to the melting and perhaps scant degradation of the low molecular weight components without significant mass loss. Looking at the endothermic range between approximately 350° C to 450° C (Figure 18A) and comparing it with the thermogravimetric (TGA) data (Figure 18B), there is a significant mass loss that corresponds to the binder components degradation. The degradation of the binder starts around 250 ºC, and its total vaporisation occurs at 500 ºC.

From the differential thermogravimetric (DTG) curve (Figure 18B), we noticed two peaks at about 385 ºC and 454 ºC. The existence and the transition between the two peaks may indicate the presence of at least two distinct components. In the first spike, there is the

degradation of the first component and sudden deceleration, possibly because of its depletion. The kinetics increases again until a second peak is reached, which might correspond to the degradation of a second component. At this last peak, the binder degradation/mass-loss rate reaches a maximum value of 11.5 %/min.

Based on the data, to remove the binder, it makes sense to establish a prolonged isothermal stage around 300 °C for the slow elimination of the binder since the degradation occurs with the kinetics of about 2%/min. Then, after a slow increase in the temperature, an isothermal stage at 500 °C seems plausible to guarantee the total elimination of the remaining binder.

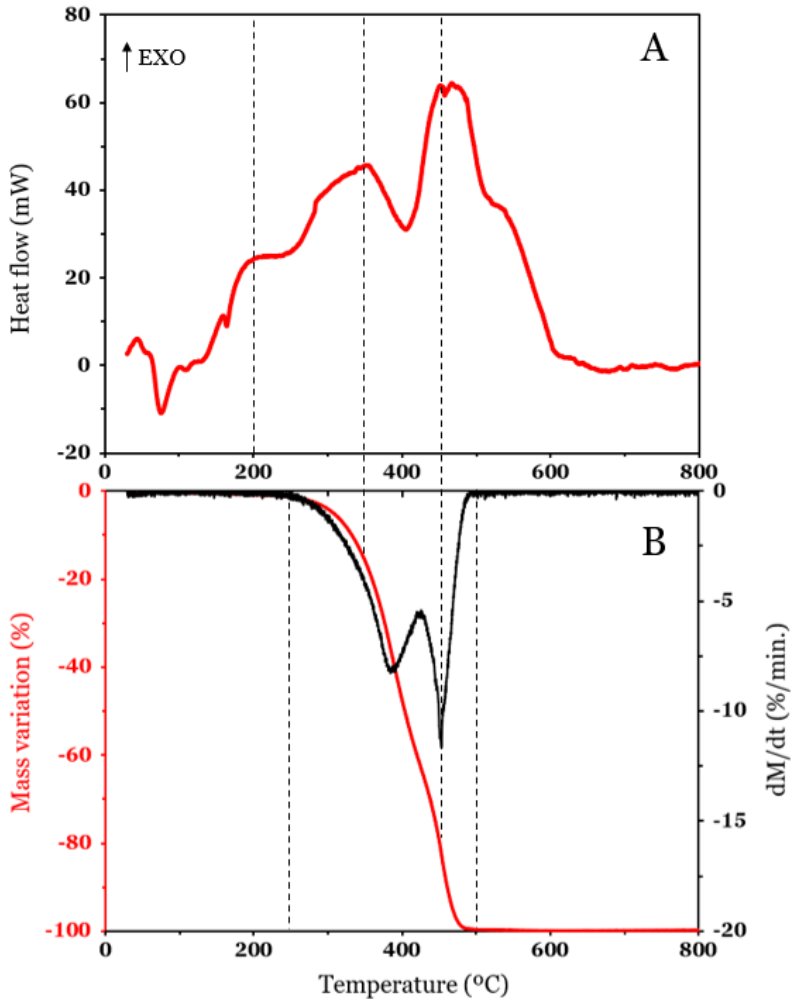

Figure 18: A) DSC curve, B) Thermogravimetric curve and its respective time derivative of mass-variation plotted against the temperature of the M1 binder.

4.1.2. Powder loading selection

The uniform mixing is achieved when the torque reaches a stable and steady state. Thus, it is relevant to conduct a careful analysis of the mixing behaviour of the mixtures. Figure 19 illustrates the complex behaviour of the SAE H13:M1 mixture for different ratios over time. Before the blends reach a stable state, we can identify two distinct zones: A and B.

In Zone A, the three curves contain several convoluted peaks that do not exceed 0.25 N.m. This region coincides, most likely, with the inertia/resistance offered by the molten polymer to the rotating blades at the beginning of the mixing. In zone B, there is a sudden increase in torque for all three mixtures. The dramatic increase is due to the sudden addition of powder which increases the viscosity of the mixtures. The maximum recorded torques were about 3.6 N.m for the 55:45 and 57:43 ratios and 4.6 N.m for the 60:40 ratio.

After approximately six minutes, the mixing torque appears to get steady for the 55:45 and 57:43 mixtures. After about 15 minutes, the torques of the two mixtures attain values of about 2.1 and 2.5 N.m without sizable oscillations.

On the other hand, for the 60:40 mixture, the mixing torque does not seem to reach the same stability as the former two mixtures. The oscillation of the mixing torque after 40 minutes is between about 3.5 and 3.9 N.m, which still corresponds to a considerable range of variation. The instability is probably due to some powder particles not being enveloped by the binder, i.e., during mixing, the blades may exert strain on either the powder-binder pair or loose powder. This phenomenon is not desirable as it directly impacts the filling of the mould cavities in the subsequent hot embossing step.

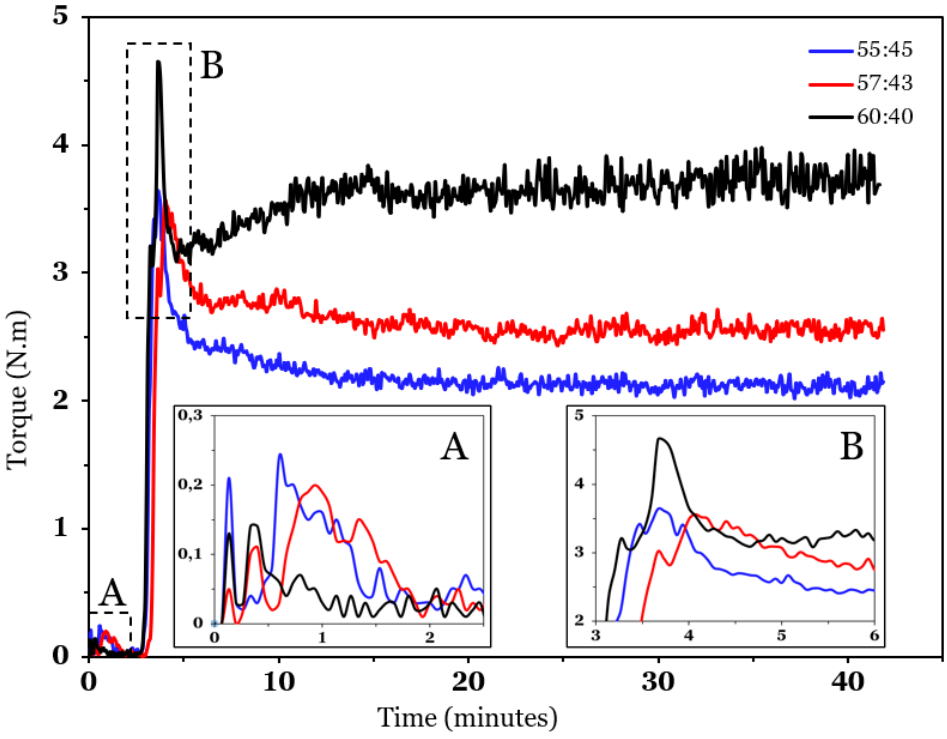

Figure 19: Torque variation over time for three different H13:M1 ratios.

Given the torque instability of the 60:40 mixture, the choice of the optimal ratio falls on the first two mixtures. Of the two mixtures, one might get tempted to choose the 55:45 ratio as it has less viscosity, i.e. the mixture would flow more efficiently into the cavities. However, the powder/binder mixtures with higher binder content will likely show a much higher shrinkage after sintering since the binder will leave more space after debinding. As we intend to minimise the remaining porosity content and shrinkage after sintering, it makes sense to opt for the 57:43 ratio mixture.

4.1.3. Visual assessment

Starting from the ideal condition found in the work of Sequeiros *et al.* [20] (220 ºC, 8 MPa, 30 minutes) and using the transparent silicon die, we tested some variations in the embossing parameters. For this, we started by increasing the holding time from 30 minutes to 45 minutes. Looking at the results illustrated in Figure 20, the green part B shows a pristine detail replication, with only a slight defect surrounded by a dashed line. The holding time increase seemed to give the mixture extra time to flow into the die cavities. Moreover, the minor and dashed defect could come from contamination of the feedstock or the silicon die.

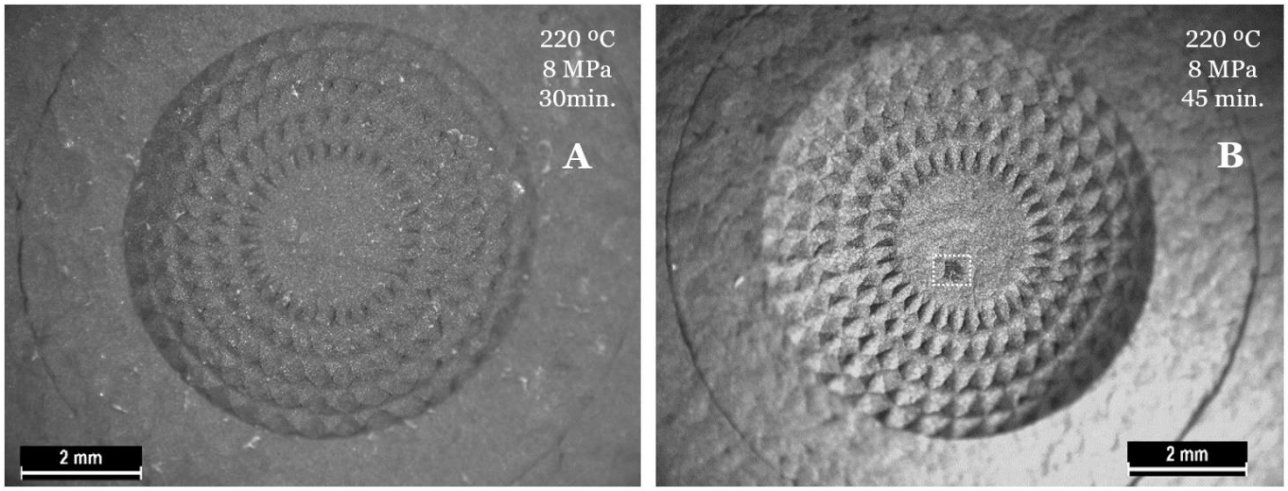

Figure 20: SAE H13:M1 parts A) original condition and B) first iteration.

Increasing the time produced good results. But, to avoid prolonging the production time, we experimented with increasing the temperature and keeping the initial 30 minutes. However, we can see from Figure 21 that the replication quality seems slightly worse compared to the first iteration. Nonetheless, we can still say that the detail replication is still reasonable. In this case, an increase of 10 ºC seemed to have less impact when compared to an increase of 15 minutes in the holding time, which may indicate that there was no significant increase in the mixture's fluidity.

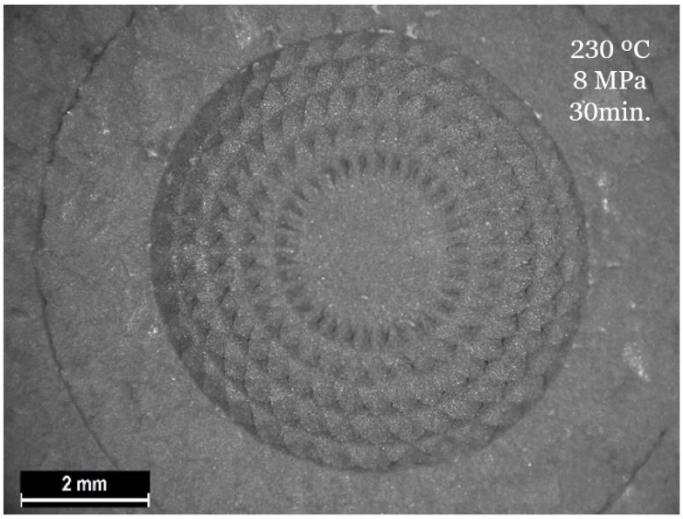

Figure 21: SAE H13:M1 part: second iteration.

Additionally, two other possibilities were then tested: the first one consists in reducing the temperature from 220 ºC to 210 ºC, maintaining the initial pressure and holding time (8 MPa, 30 minutes); the second one consists in cutting down the embossing pressure from 8 to 5.33 MPa, maintaining the initial temperature and holding time (220 ºC, 30 minutes). Unfortunately, as we can observe from Figure 22A, the replication deteriorated notably compared to the initial conditions. The decrease of 10 ºC might have been enough to reduce the mixture's viscosity significantly.

The result of the fourth iteration is presented in Figure 22B. In this particular condition, the drastic pressure reduction showed a strong impact, as there was no replication of any detail. The result is not perplexing since the viscosity of these thick mixtures is poor when there is little to no outside pressure.

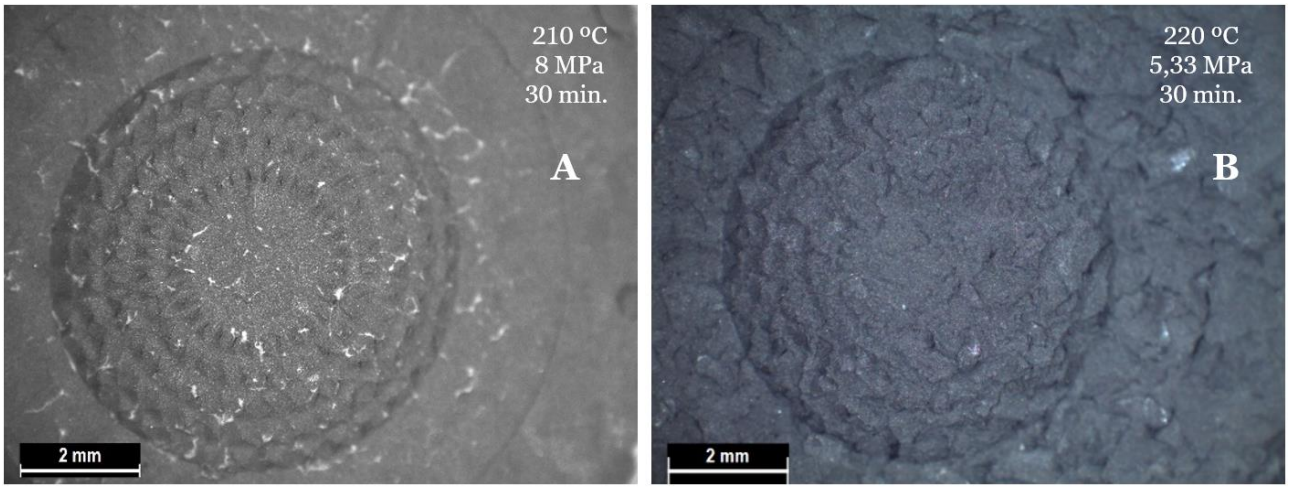

Figure 22: SAE H13:M1 part: A) third and B) the fourth iteration.

Following the analysis of the green parts, only the sample in Figure 20B (220 ºC; 8 MPa; 45 minutes) proceeded to the sintering step, as it was the one that visually demonstrated the best replication of detail. From Figure 23, the sample was relatively well sintered. The presence of small debris in the centre of the sintered part (Figure 23B) resulted from

presumably careless handling of the green part, which means that upon sintering, those particles will inevitably become attached to the component. The linear contraction was 12.67%.

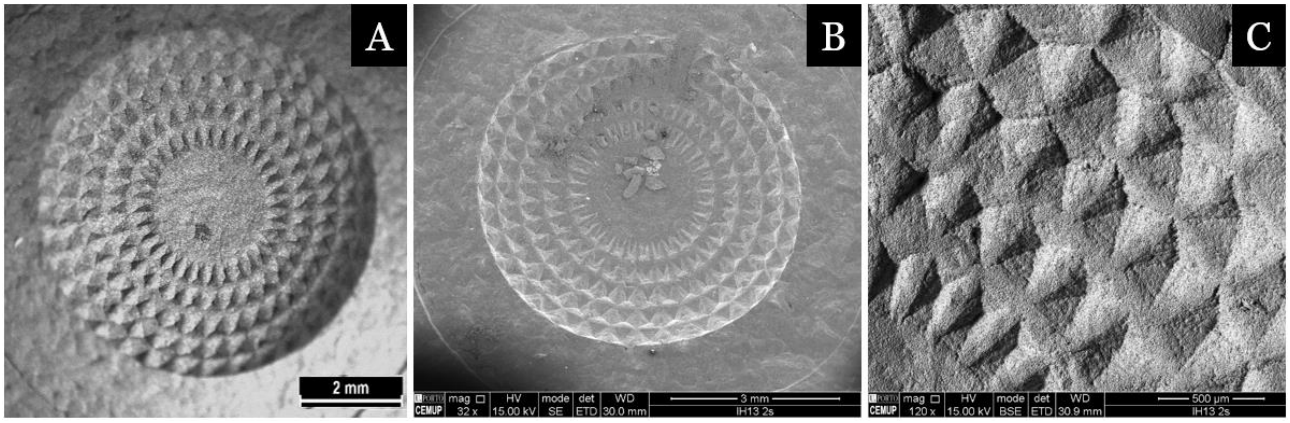

Figure 23: A) Green part from Fig.18A, SEM image of the B) sintered component and a C) magnification of some details.

4.2. Material extrusion

4.2.1. H13 filament characterisation

Figure 24 shows the appearance of the filament and a magnification of the powder particles distributed on the filament. The filament has slight defects on its surface, such as straight parallel marks in the direction of the filament length and black spots. These two defects are most likely due to the extrusion of the filament during its production. Presumably, it will not impact the printing process of the part.

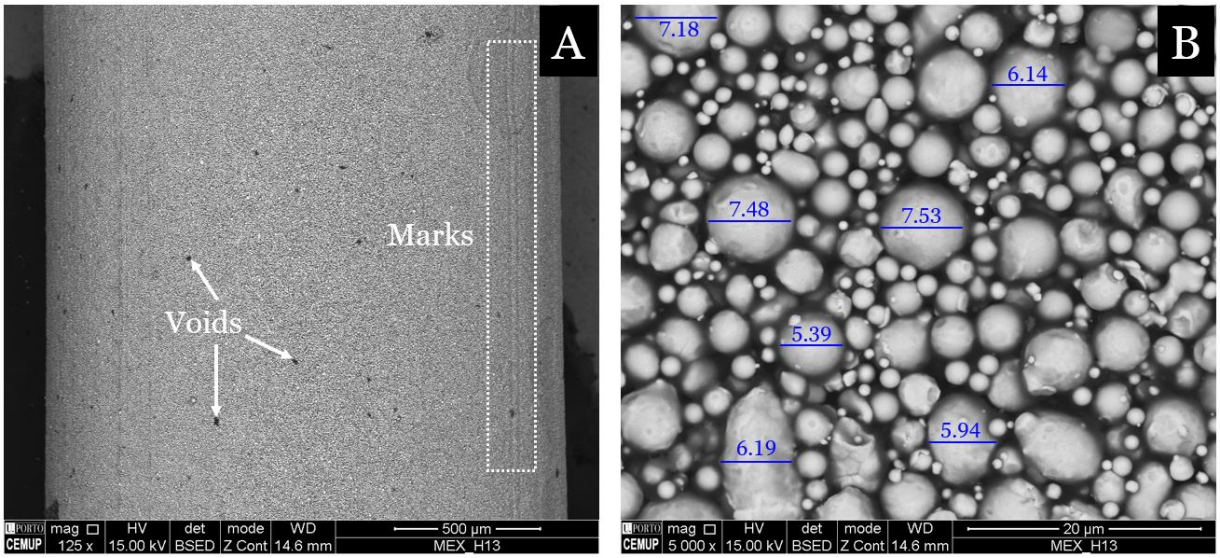

Figure 24: SEM images of the A) manufacturer's filament and B) magnification of the particles with some measurements (in µm).

As for the powder, overall, the particles have a spherical morphology, much more regular when compared with the previous mixture's powders and the satellite phenomenon seems to be non-existent. Unfortunately, no particle size distribution curves were built for the powder particles. However, using a swift image analysis software such as *ImageJ* and measuring the largest particles, we found that the biggest particles (in Figure 24B) did not exceed 10 micrometres. Seemingly, this statement needs experimental corroboration through a particle size distribution (PSD) analysis of the original powder using more appropriate techniques, such as laser diffraction. Moreover, many more image fields would be mandatory to substantiate the image analysis methods.

By analysis of the DSC curve (Figure 25A), the binder present in the filament shows two endothermic peaks before 60 ºC and a tiny valley between 145 and 152 ºC. The first peak corresponds, most likely, to the melting of the binder. The second peak might correspond to the degradation of a low molecular weight component in meagre contents [20].

Looking at the thermogravimetric data (Figure 25B), the binder present in the filament appears to start its degradation at 180 ºC. During the test, the binder undergoes three stages until its total degradation at about 480 ºC. We can also notice two peaks regarding the mass loss rate (black curve).In the first stage, between 180 and 315 ºC, the binder loses about 60 per cent of its mass. The kinetics of maximum mass loss reaches about 7,5%/min at around 225 ºC. In the second stage, between 315 and 435 ºC, the binder does not undergo significant mass variation. It indicates that the total degradation of at least one component occurred before the plateau. The gap between the two peaks is a lot wider when compared to the previous M1 binder. Thus, it suggests that the two compounds have distinctive degrading temperatures. The remaining binder evaporates in the last stage, above 435 ºC, and reaches a maximum mass loss rate of about 18,75%/min at about 465 ºC. From then on, there is a deceleration due to the fast depletion of the remaining binder. We can consider that the binder is depleted at 475 ºC.

From these results, it makes sense that the thermal debinding of the filament should, at least, contemplate an initial isothermal stage between 180-315 ºC and another isothermal stage between 435-475 ºC. Considering that there is a more significant amount of mass to be degraded (60%) in the first stage compared to the second stage (40%), the duration should also be slightly longer. However, during the slow heating of the green parts, we know that the degradation of the binder will occur, i.e., when the parts reach the temperatures of the isothermal stages, their duration will not need to be very long. Having said this, we stipulated isothermal steps with maximum durations of 1 hour.

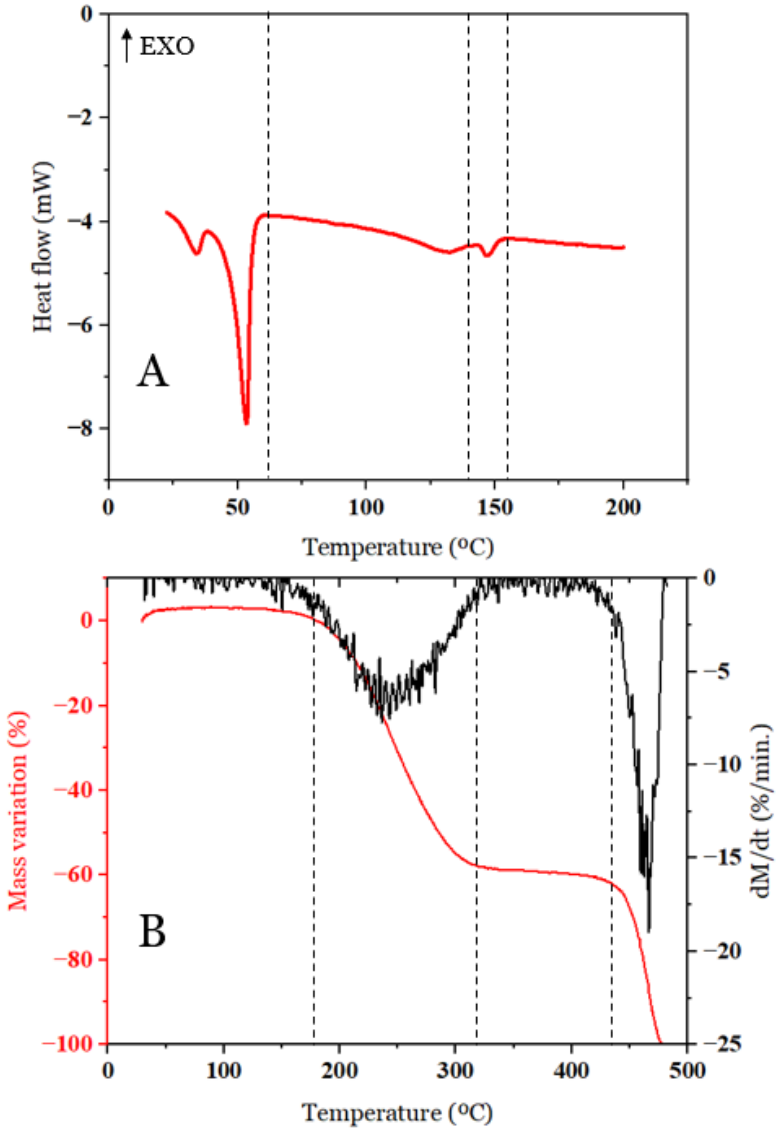

Figure 25: A) DSC curve, B) Thermogravimetric curve and its respective time derivative of mass-variation plotted against the temperature of the filament.

4.2.2. Visual assessment

Figure 26A shows the result of the green part produced in the ME process. We can easily observe that the ME equipment fails to replicate the geometry's details. The struggles to replicate those details with the material extrusion were likely to appear since the line width (corresponds to the nozzle's diameter) deposition applied was 0.4 mm. As shown in Figure 26B, the geometry has details far below that thickness. In a way, the poor replication of the geometry details was not surprising, highlighting the limitation of this AM equipment/technology.

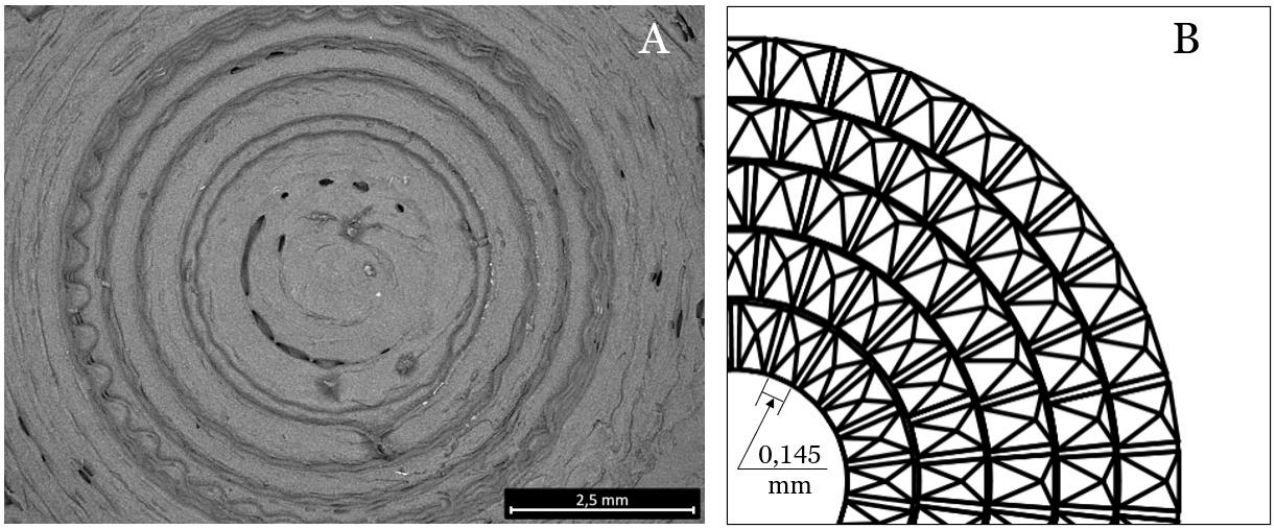

Figure 26: A) Part produced by material extrusion and B) the width of the smallest detail.

4.3. Hot embossing of the manufacturer's filament

4.3.1. Visual assessment

To efficiently compare the green bodies and discern the differences between the different DOE conditions, we assembled the images as shown in Figure 27.

By analysing Figure 27, it is immediately noticeable that the level of detail replication improves substantially with increasing temperature. In particular, the increase in temperature from 190 to 200ºC seems to influence detail reproduction significantly. This observation makes sense as the increase in temperature turns the feedstock less viscous. When the mixture becomes less viscous, it has considerably more ease in flowing and filling the cavities of a mould. One may question the temperatures selected for the DOE, as these are around the beginning of the mass loss of the binder. However, for the sake of the replication quality, we consider that imposing a slight early degradation of the binder (at least one of its components) seems to be an acceptable trade-off.

Regarding the pressure, although this is a relevant factor in pushing the mixture into the cavities, only a slight improvement from part **E** to part **F** can be noted. It can be said that pressure seems to have little impact on the detail replication enhancement. Perhaps a difference of 2.67 MPa is too low to detect its influence.

Moreover, an increase of 15 minutes in holding time does not seem to have much impact on the detail replication. The most noticeable differences are only between samples **A** and **C**. So, the complete filling of the cavities has likely occurred within 30 minutes.

Finally, it is possible to detect a minor defect in the centre of the parts produced at 210 ºC. These defects come from the scratches left in the silicon die mould during cleaning after parts production.

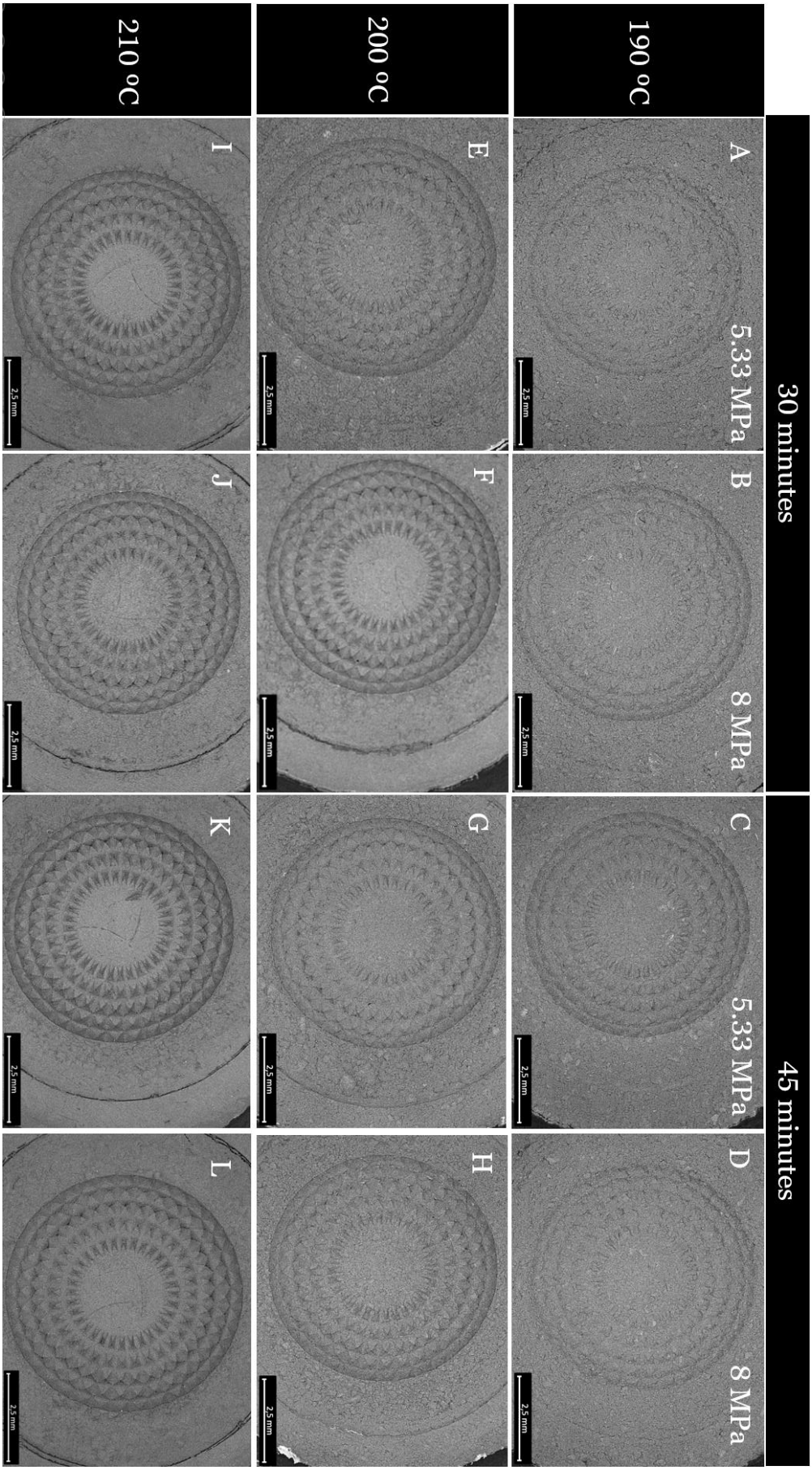

Figure 27: Hot embossed parts from the ground filament.

To better understand the interaction of the three hot embossing parameters, we will assign qualitative values to the replication quality of the different green parts samples. For that, we defined a scale of -1, 0 and 1. The negative one (-1) indicates that the sample did not replicate or partially replicated some of the details; The zero (0) indicates that the sample replicated all or almost all the details but without a clear definition of the edges of the pyramidal cavities; The one (1) indicates that the sample replicated all the details and displays all the edges of the pyramid cavities. The following table contains the quality values attributed for each condition based on the visual judgement of Figure 27.

Table 8: Quality values attributed to the samples.

Temperature (ºC)	Pressure (MPa)	Time (min.)	Quality
190	5.33	30	-1
	8.00	30	-1
	5.33	45	0
	8.00	45	-1
200	5.33	30	0
	8.00	30	1
	5.33	45	0
	8.00	45	0
210	5.33	30	1
	8.00	30	1
	5.33	45	1
	8.00	45	1

The next step will be the construction of interaction graphs between the different variables. For that purpose, we defined temperature, pressure and holding time as the variables and quality as the response. In Figure 28, it is possible to observe the paired interaction plots of the three variables studied in the hot embossing: temperature, pressure and holding time. It should be noted that this is a very subjective evaluation and may produce slightly different results if a different quality grade is assigned to each condition.

Looking at the graph of temperature against pressure, we can see that the average quality improves significantly with increasing temperature. The increase in pressure from 5.33 to 8.00 MPa had little effect since there was no abrupt change in the slope of the curves. The same conclusions are valid regarding the pair temperature versus time. The improvement in replication quality improves with increasing temperature, regardless of the holding time. These observations allow us to infer that temperature is the most preponderant factor.

As for the pressure versus time interaction, the average quality for a 30 minutes holding time increases slightly with the pressure increase. However, this trend seems to invert with a holding time increase of 15 minutes (negative slope). This behaviour is a bit confusing since increasing the holding time would theoretically mean an increase in the time for the filling of the mould cavities. The parts that contributed to this odd result were the 190 ºC/5.33 MPa/45 min. (Figure 27C) and 200 ºC/8 MPa/30 min. (Figure 27F) part. That said, it would

be necessary to produce even more samples under the same conditions to ascertain the reproducibility of the results.

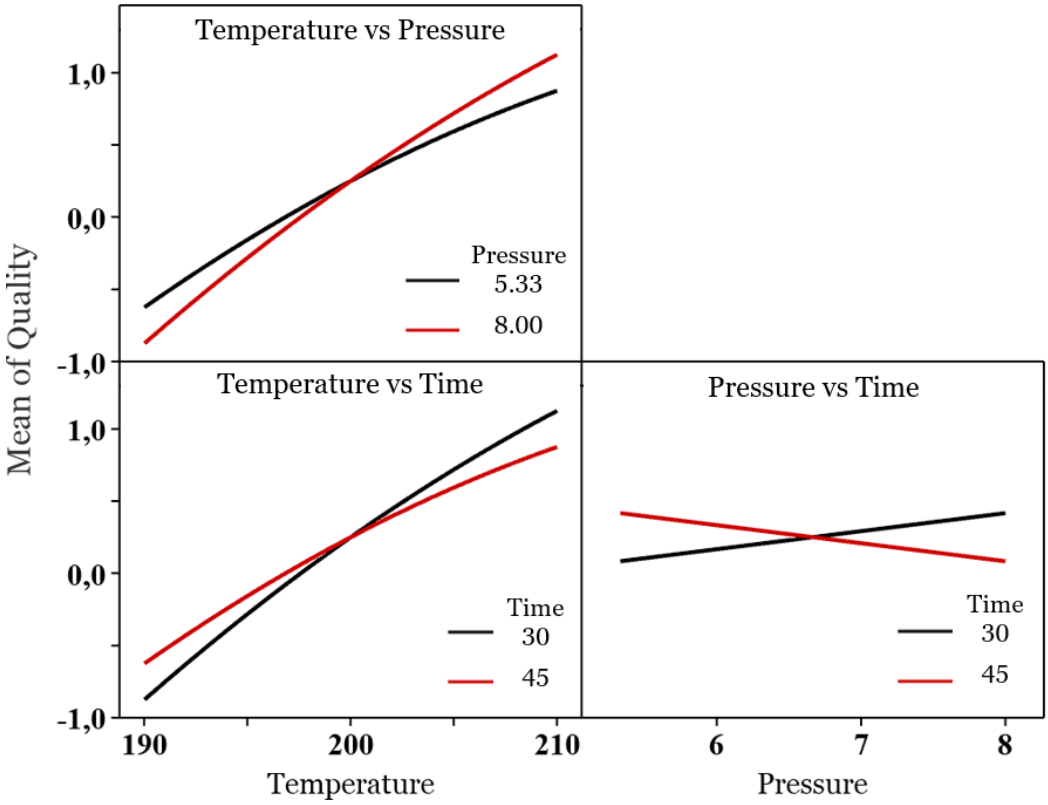

Figure 28: Interaction plots between the three parameters: temperature, pressure and holding time.

The choice of the parts with the best replication of detail for further sintering will fall on those parts that were assigned a rating of one (1), i.e. green parts produced with 200 ºC/ 8 MPa/ 30 min. and those produced at 210 ºC. To support the decision-making, it seems appropriate to have other criteria, like the linear deviations of the green parts from the silicone rubber die. Knowing that the silicone mould geometry has a diameter of 6.61 µm, the modules of the calculated deviations are displayed in Table 9.

Table 9: Linear deviations of the selected samples from the silicon rubber die.

Temperature (ºC)	Pressure (MPa)	Time (min)	Measured diameter (µm)	|Deviation (%) |
200	8.00	30	6.59	0.30
210	5.33	30	6.58	0.45
	8.00	30	6.62	0.15
	5.33	45	6.73	1.82
	8.00	45	6.67	0.91

From the deviations, the component 210 ºC/8 MPa/30 min was selected for the sintering step. We can observe from Figure 29 that overall, the sintering seems to have been successful as the part retained the replication details and showed a linear contraction of 12.84%.

Although, the part could use some superficial polishing, we can assert that at least the visual result far exceeds the one obtained in AM.

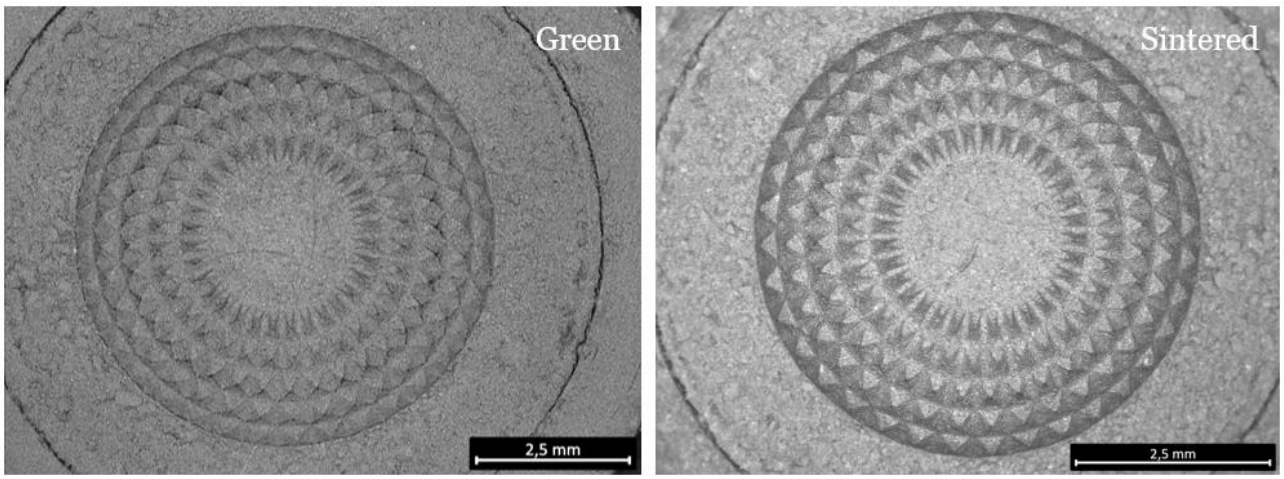

Figure 29: Green and sintered 210 ºC/8 MPa/30 min. part.

4.4. Mechanical, microstructural characterisation and heat treatments

In this section, we will first present the results regarding the components produced by AM and then proceed to the sintered hot embossing samples.

4.4.1. Additive manufactured parts

After sintering in *Sinter 1*, we can observe from the microstructures of Figure 30A that the components produced by AM still have some residual porosity. Additionally, it is possible to identify dark marks aligned in one direction on the periphery of the cubes (Figure 30B).

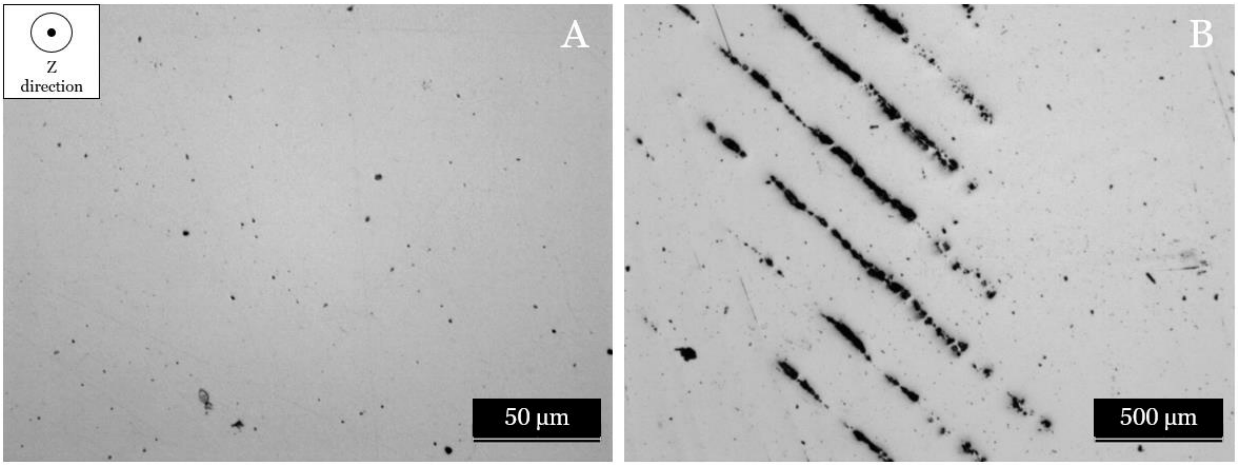

Figure 30: A) Pores and other B) other microstructural defects detected in MEX samples debinded and sintered in *Sinter 1*. Z direction refers to the direction aligned with the printing nozzle.

We can assume that these marks are voids that derive from defective material deposition during printing, i.e. when the print head deposits the filament, it may sometimes not deposit enough material at a trajectory change. Thus, the gap between those paths will remain empty. During sintering, the bonding of the deposited tracks will not occur. This type of flaw was found in all cubes and seems like a common defect in products produced by ME [47,54].

As for the component with the intended geometry and not sintered in *Sinter-1*, the pore shape (Figure 31A) is more irregular, and seems different from the ones Figure 30A. It is also noticeable the lack of sintering of some powder particles (dashed in Figure 31A). The issues may stem from the thermal cycles of debinding/sintering and the poorly controlled atmosphere. We do believe that these cycles may not be the ideal ones, specially the sintering temperature. From the literature [55], the authors observed that higher sintering temperatures yielded denser parts with less non-sintered particles, and more spherical pores. So we assert that a better sintering atmosphere and higher sintering temperatures could improve the overall microstructure. Moreover, from Figure 31B and C, we can see the cross-section of the dark marks (voids) and their uniform distribution across the specimens.

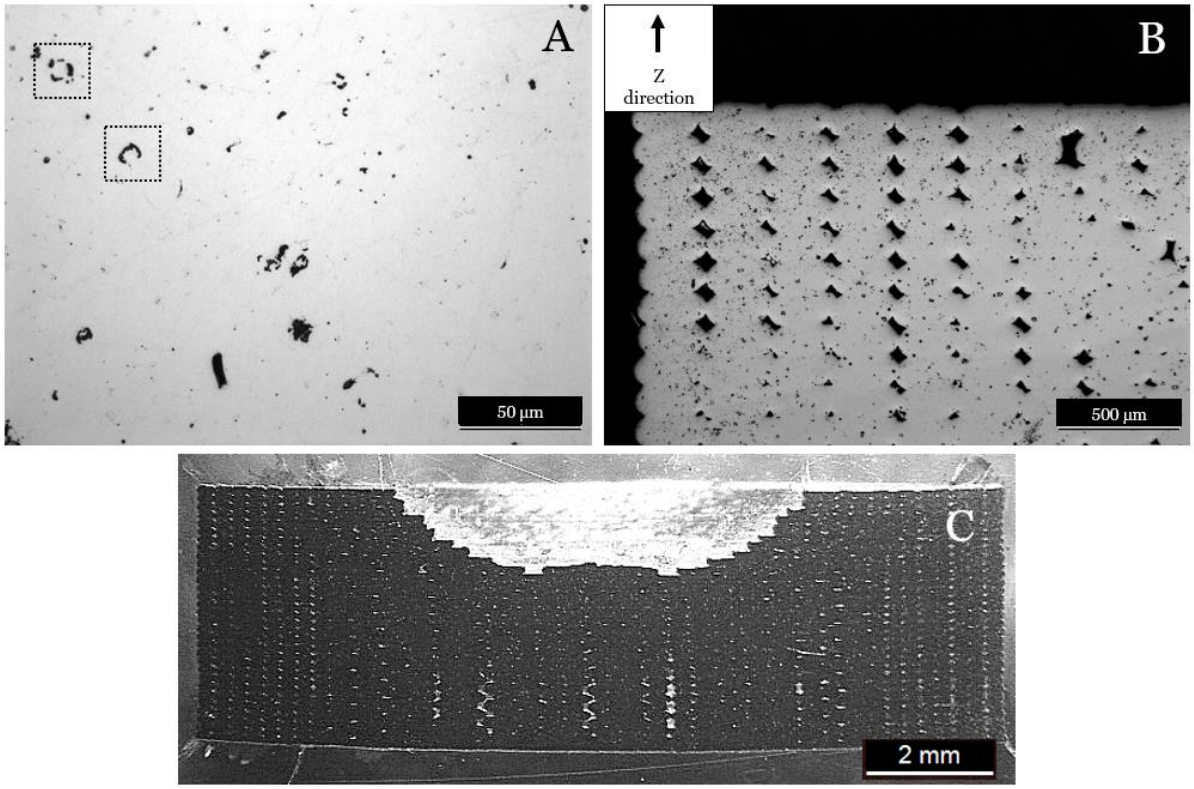

Figure 31: A) Pores, lack of sintering (dashed), other B) microstructural defects detected in the MEX component that was not sintered in *Sinter-1.* C) corresponds to the cross-section of the sample.

In Figure 32 we can observe a microstructure of the as-sintered parts. According to *Costa et al.* [47], this is a martensitic microstructure with coarse grains and porosities. To obtain a martensitic structure, sufficiently fast cooling would be necessary to avoid the formation of equilibrium structures. Generally, during sintering, cooling is usually slow. But

unfortunately, the thermal cycle of the *Sinter1* furnace is not known, so it is not possible to make a conclusion regarding the cooling rate. However, given that the SAE H13 tool steel is a highly alloyed and air-hardenable steel, the authors' assertions regarding the presence of martensite hold some grounds.

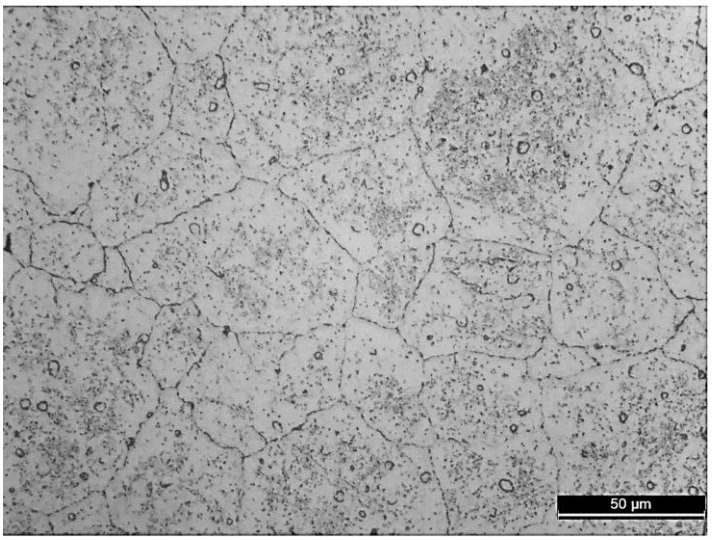

Figure 32: Microstructure from optical microscopy of as-sintered and etched SAE H13 tool steel.

The SAE H13 steel cube produced by ME showed a hardness of about 375 ± 5 HV, which is well below what is expected for tool steel (400-650 HV) ([56]). After austenitising and quenching, a hardness of 426 ± 17 HV was achieved. In Figure 33 we can see a microstructure of the quenched sample. It is possible to state with some certainty that martensite is present as little needle-like constituents.

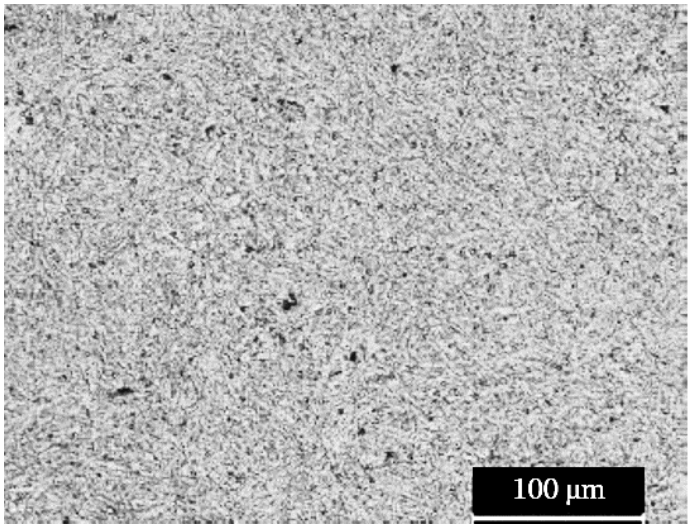

Figure 33: Quenched and etched SAE H13 microstructure (optical microscopy).

As the quenching heat treatment is usually followed by tempering, we studied briefly the behaviour of the SAE H13 under different tempering temperatures. Some microstructures regarding the microstructural evolution of SAE H13 steel obtained by MEX is shown in Figure 34.

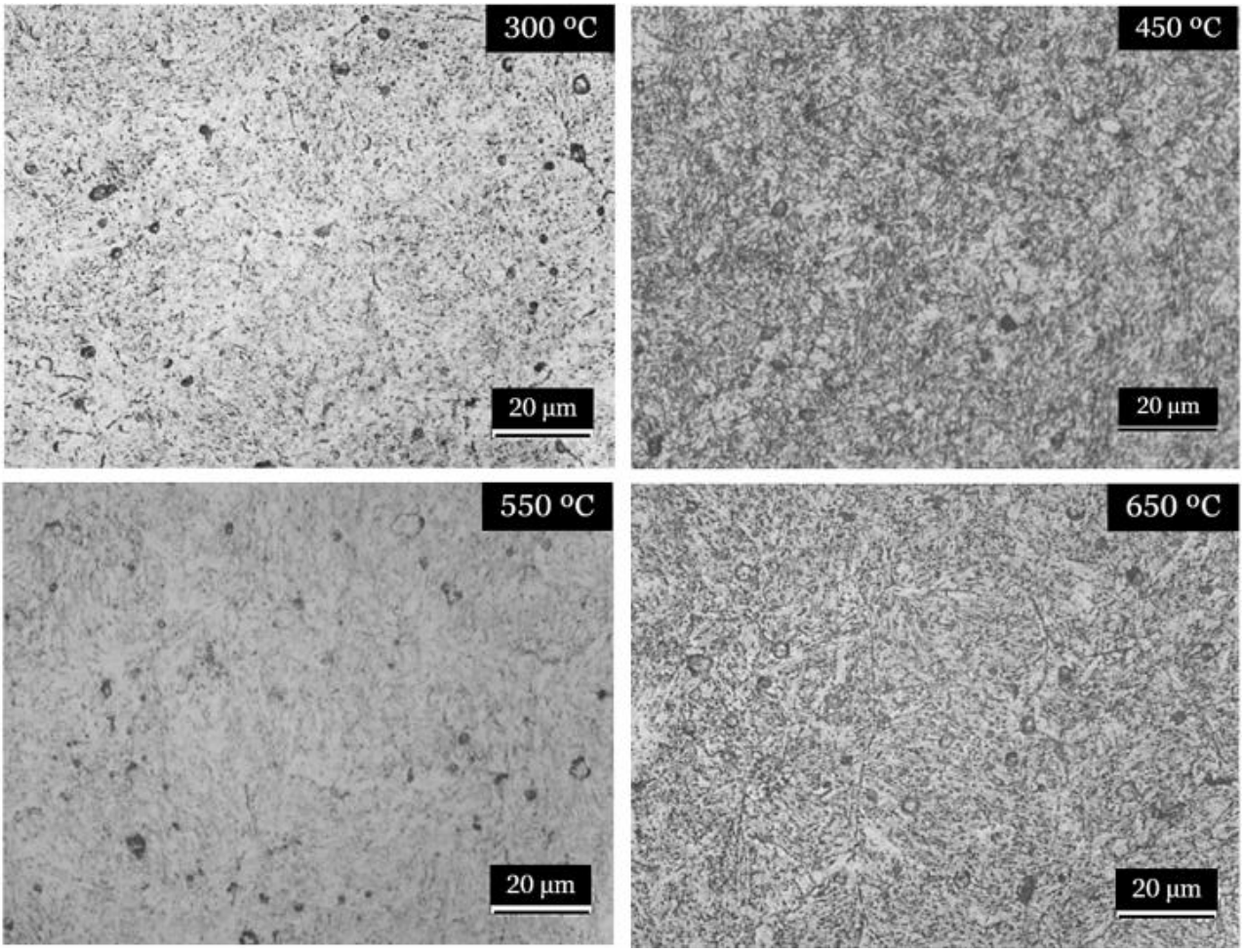

Figure 34: Etched microstructures from optical microscopy of SAE H13 after quenching at 1020 ºC and tempered at different temperatures (300-650 ºC).

Looking at the 300 ºC tempered microstructure (Figure 34(300 ºC)), we did not notice any noteworthy differences compared to the quenched state. However, there is an increase in hardness from the initial quenched state (426 HV to 440 HV). This increase is probably due to the precipitation of transition carbides such as $Fe_{2,4}C$, which will hinder the movement of dislocations [57].

Above 400 ºC, steels are characterised by the formation of cementite and ferrite. In addition, depending on the temperature, the spheroidisation of carbides will occur. In this particular case, the formation of some of the equilibrium phases seems visible at 550 ºC (Figure 34 (550 ºC)) [57]. Furthermore, the measured hardness of 304 $\pm$ 8 HV substantiates our observations.

At 650 ºC (Figure 34(650 ºC)), the microstructure seems strongly dominated by ferrite and cementite. In addition, it is already possible to observe the spheroidisation of some carbides. A relevant aspect to note is that steels with considerable chromium, molybdenum, vanadium and tungsten in their composition, such as SAE H13, are prone to form alloyed carbides at around 500 ºC [57]. Looking again at the microstructures (Figure 34), it is likely that this event occurred around 450 ºC.

In the graph in Figure 35, we can see the overall progression of the hardness of the parts produced by ME for different tempering temperatures. By looking at the behaviour of the curve, during tempering below 500 ºC, the steel presents a remarkable resistance to softening. At 450 ºC, this steel slightly increased its hardness. This phenomenon, called secondary hardening, is common in hot-work tool steels. Secondary hardening is characterised by intense precipitation of fine, semi-coherent carbides within a given tempering temperature range. By glancing at Figure 34-450 ºC, the microstructure conveys an impression of thinner carbides compared to the other tempering temperatures. In appreciable contents, this phenomenon is recurrent in steels with molybdenum, tungsten, or vanadium [56,57].

For temperatures above 500 ºC, the hardness decreases dramatically as the fine precipitates begin to coarse and become more coherent with the matrix. Moreover, when the matrix is depleting carbon and the carbides spheroidises, it becomes ferritic, i.e., softer [58]. This event is more noticeable in the sample tempered at 650 ºC (Figure 34 (650 ºC)).

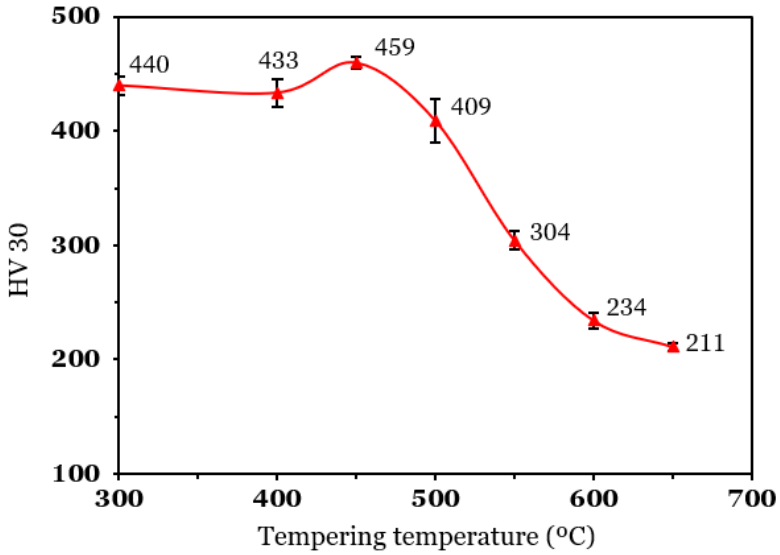

Figure 35: Hardness evolution of AMed SAE H13 steel under different tempering temperatures.

Moving on to the tensile tests, the results presented in Figure 36 are representative of the specimens tested. Here the tensile specimens were tested in their original as-built condition and the heat-treated condition that yielded the highest hardness (quenched and tempered at 450 ºC). In the as-built state, SAE H13 has a yield strength of about 760 MPa, a tensile strength of 1177 MPa and an elongation of less than 2%. In the heat-treated state, SAE H13 demonstrated a yield strength of about 947 MPa, a tensile strength of 1014 MPa and an elongation of less than 1.5%. Looking at the right side of Figure 36, one can see that in both cases, the mechanical properties were below that found in the literature [50]. It is worth noting that more tests would be necessary to validate the results since the distribution of possible defects is stochastically dependent, and three test specimens are not statistically representative of a population.

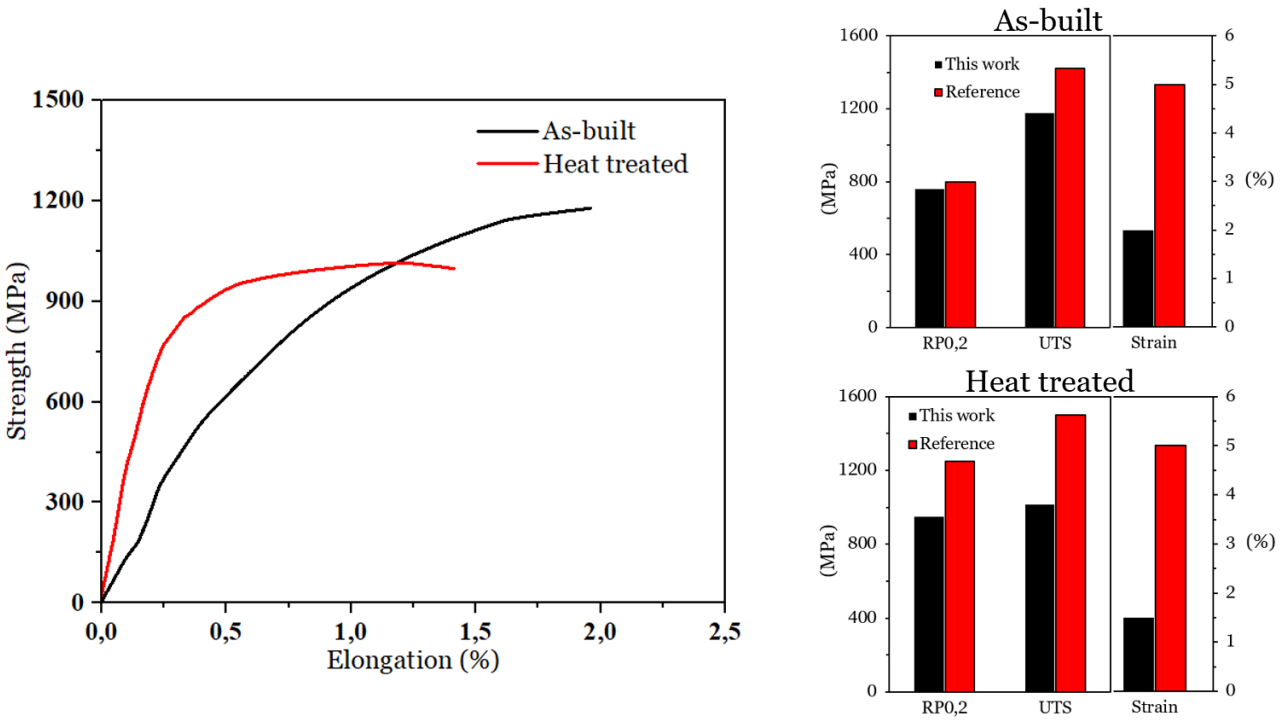

Figure 36: Tensile results from the AMed specimens.

The presence of defects such as those observed above (in Figure 30B) has likely contributed to this. Another reason for the subpar tensile performance might be related to the rupture mode of the tensile specimens. We can see from Figure 37 that the tensile specimens ruptured in a peculiar way. It appears that some deposited metallic tracks did not bond laterally at all after sintering. So we believe that there were "multiple" separate tensile tests being carried at the same time, which again risks the result's credibility.

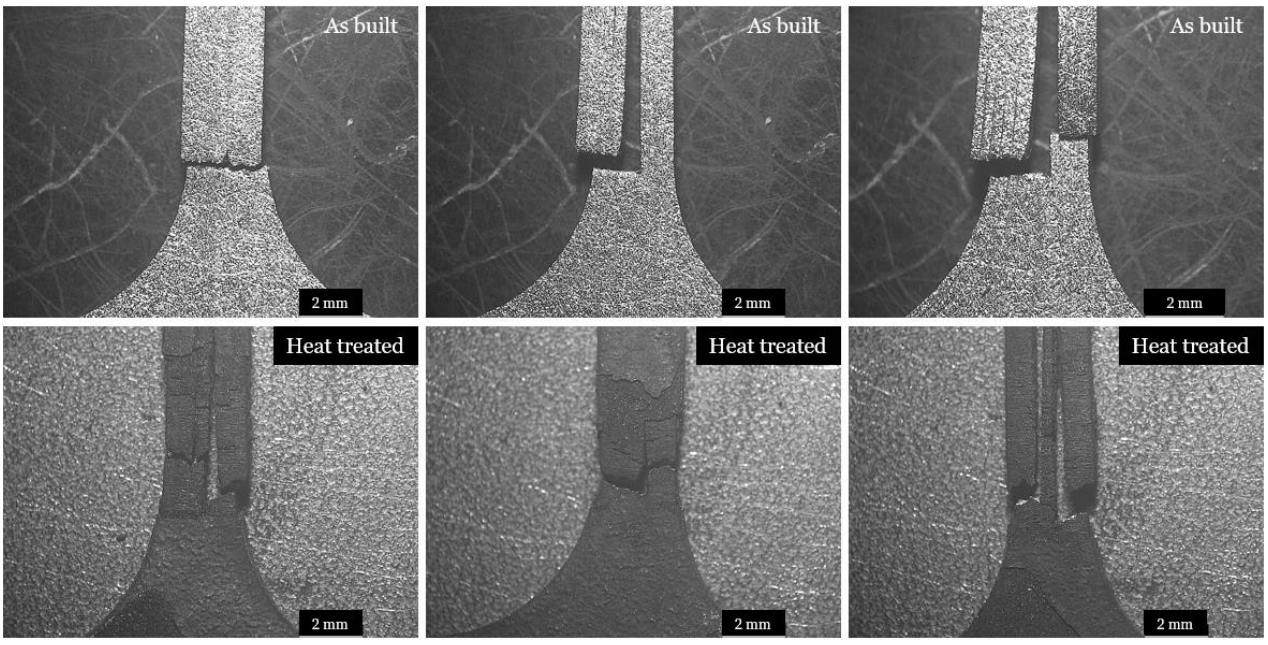

Figure 37: Representative images of the tensile specimens after the tensile test (rupture zone).

Another staggering detail is that the ultimate tensile strength of the heat-treated specimen is below the as-build condition. The most plausible hypothesis is related to the fragile, porous and poorly adherent oxides formed during the heat treatments and visible in Figure 37 (Heat treated). As the specimens have a reduced thickness, the oxide has likely proliferated and consumed part of the metallic cross-section of the tensile specimens. This inevitably leads to a much poorer tensile performance than expected.

4.4.2. Hot embossing parts

The microstructure of the SAE H13:M1 (Figure 38A) component shows a microstructure with a considerable amount of porosity. In addition, the specimen presents large cracks and some large pores that are impossible to ignore (Figure 38B). The reason for the formation of these defects might be related to the powder morphology. The powder used in SAE H13:M1 mixture possesses an irregular shape, typical from the water atomized powders. Thus, it results in a broad pore size distribution which could inhibit sintering [59]. Although the final purpose of these components is for hot engraving of geometries in polymeric materials, we believe that cracks and macroporosity will contribute to diminishing the component's lifetime.

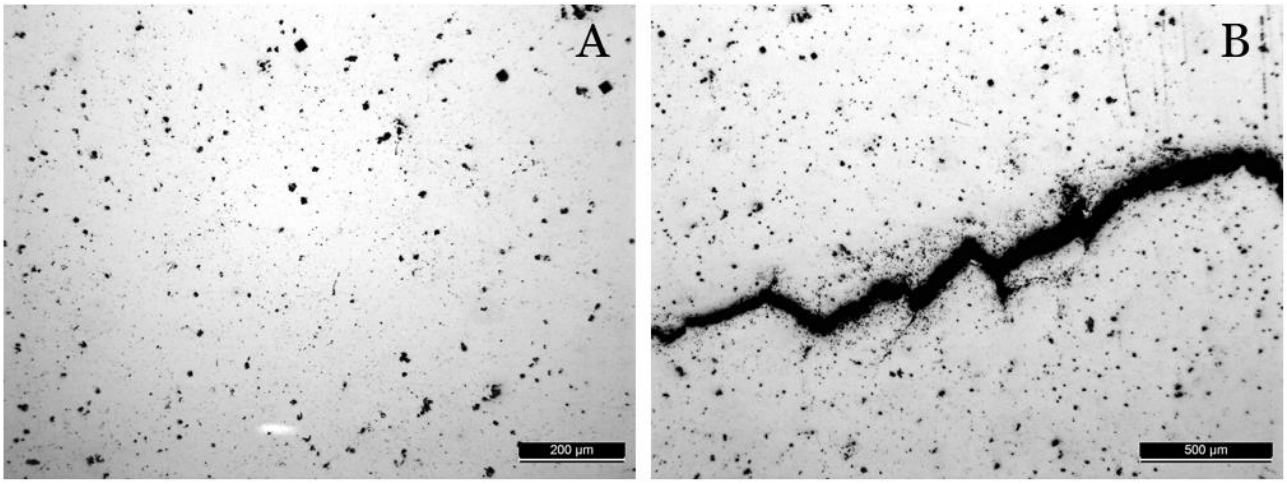

Figure 38: A) Microstructure of the component produced with SAE H13:M1 mixture and a B) crack in the centre of the component.

The hot embossing parts produced with the filament and not sintered in *Sinter-1* (Figure 39) show a lot of porosity and non-sintered powder particles. The porosity and lack of sintering indicate that the sintering conditions (poor control of the sintering atmosphere and sintering temperature) used are not the most suitable. Comparing the two microstructures (Figure 38 and Figure 39), we find a paradoxical aspect: the component obtained by hot embossing of the filament and sintered at a higher temperature showed non-sintered particles. The reason may be related to the different furnaces used for sintering. The furnace used to sinter the SAE H13:M1 component can reach higher temperatures and might have sintered the component at a higher temperature than programmed. On the other hand, the furnace used to sinter the part obtained by hot embossing of the filament struggles more in

reaching and stabilising at high temperatures (above 1000 ºC). We believe that the temperature of the sintering process may have been considerably below the programmed temperature (1250 ºC).

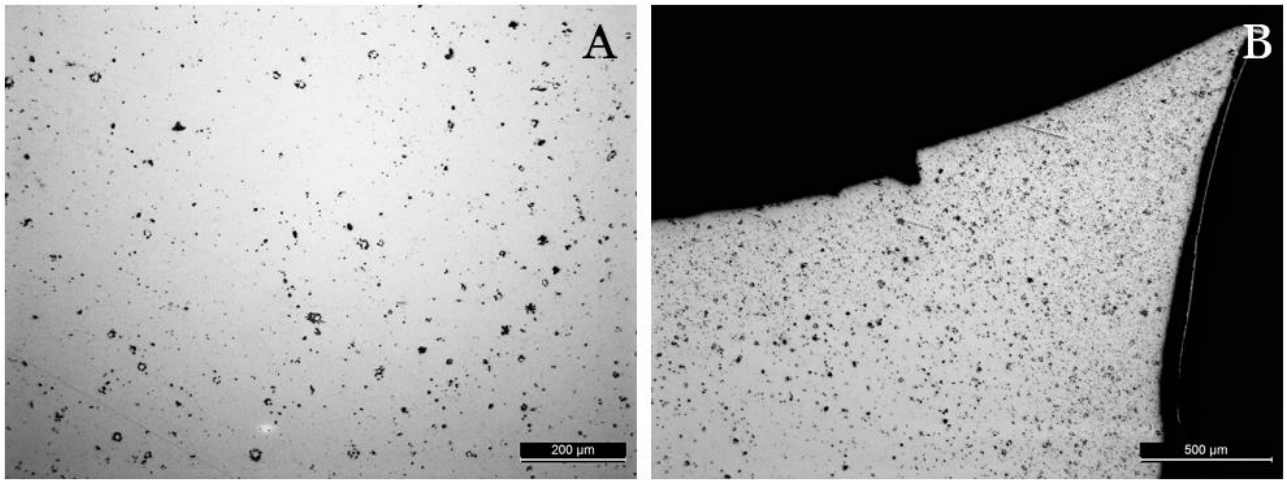

Figure 39: Microstructures of the component produced with the filament in the A) centre and the B) edge.

If we zoom out the microstructure, we can see from Figure 40 that this type of component has deformed walls. But this phenomenon was somewhat expected since it was a component shaped with a silicone rubber die. The silicon rubber, under compression, will deform towards the powder to binder granulate, which is still in the process of compaction. Assuming that the component could be employed in the industry, they would require grinding and finishing processes after production.

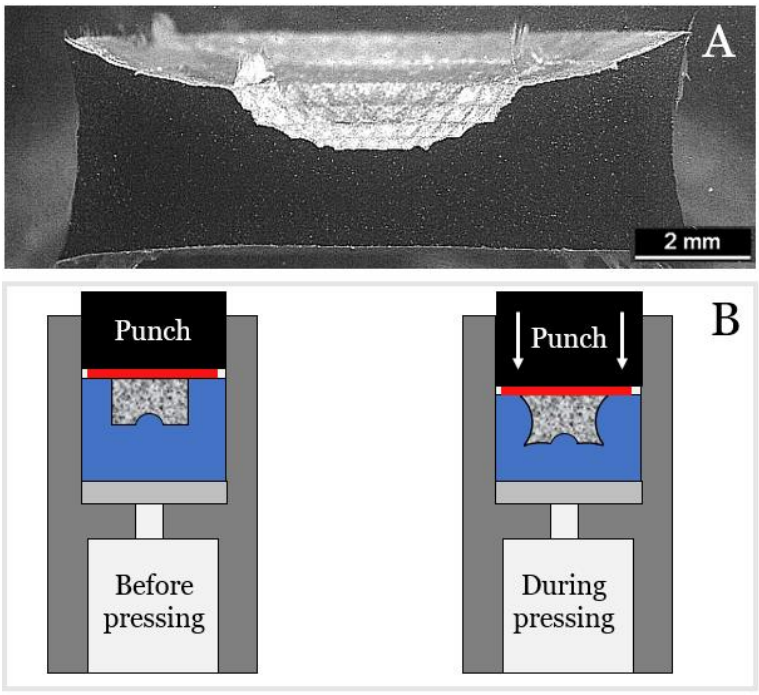

Figure 40: A) Magnifying glass image of the cross-section of the component produced by hot embossing and B) deformation of component's walls.

As for the mechanical properties, one can see in Figure 41 the comparison of microhardness between the different samples. In general, there was an increment in the hardness of all the components after the heat treatment. The "MEX *Sinter-1*"(cube obtained by MEX and sintered in *Sinter-1*) is the one that presented the highest hardness in the as-sintered state compared to all the other components sintered with cycles created by us. This fact is not unsettling since the sintering conditions of *Sinter-1* are presumably better tailored and more controlled.

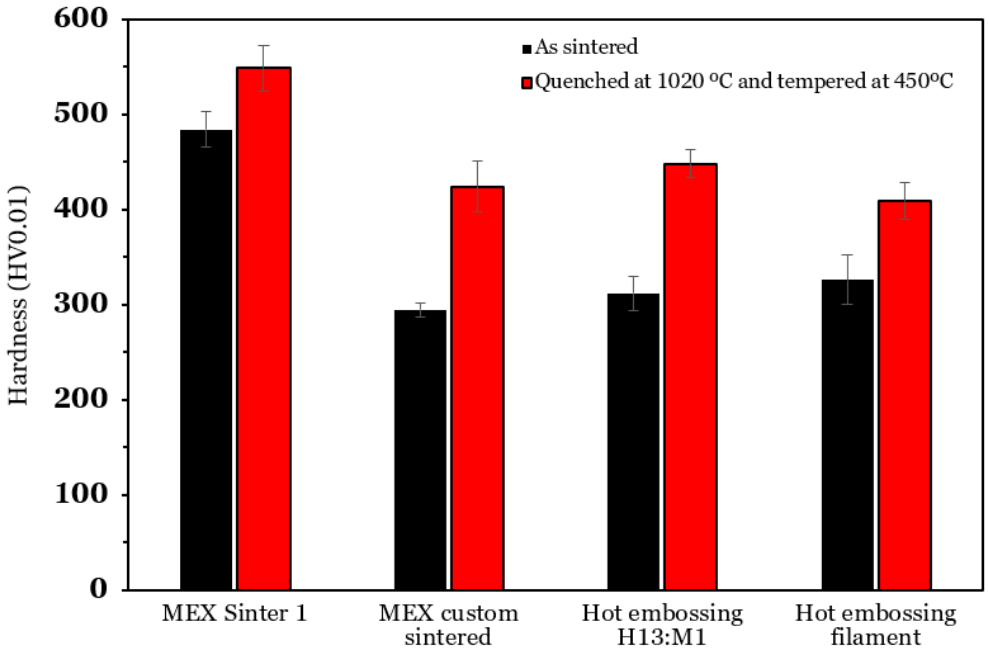

Figure 41: Hardness comparison of the components produced under different conditions.

If we compare specifically the "MEX *Sinter-1*" and the "MEX custom sintered", we can observe that although the AM was part of the processing of the components, the post thermal processing played a preponderant role in the difference in hardnesses. In fact, "MEX *Sinter-1*" demonstrated a hardness of about 64% higher than "MEX custom sintered". The discrepancy may originate not only from the sintering temperature but also from the subsequent isothermal stage at 600 °C. In the same way that a tempering at 600 ºC was responsible for softening after quenching, an isothermal treatment at 600 ºC after sintering corresponds to subcritical annealing and an inherent softening [60]. One may question the relevance of this annealing cycle since the purpose is to obtain components for hot working applications.

Regarding the other two conditions, the component obtained by hot embossing the filament showed similar hardness compared to that obtained with the SAE H13:M1 mixture. However, we can notice that the hardness increment of the "hot embossing filament" after heat treatment was slightly lower when compared to the "Hot embossing H13:M1". The increment differences stem from several reasons since they were heat treated on different occasions. Those could be fluctuations in the autenitisation temperatures, quenching method, and tempering temperatures.

4.5. Brief comparison of the manufacturing processes

After seeing the final results, it is opportune to do a very brief side-by-side comparison of the parts obtained in the different manufacturing processes and their comparison with the original metallic mould. Looking at the Figure 42, we can comfortably say that the part produced by AM was the one that presented the worst result.

Unfortunately at this moment, it is unlikely for the AM printer (*Metal X*) to reproduce the desired details. No matter how well one parameterizes the printing process, the nozzle's diameter will always remain the bottleneck of the equipment.

As for the parts produced by hot embossing (Figure 42C and D), they retained the main details of the silicone rubber die. Obviously, the surface quality cannot be compared with the initial mould (Figure 42A), as the silicone rubber die is derived from the metallic mould. In this case, as it is an insert to produce optical components, the rough surface quality characteristic of hot embossing parts may be undesirable. But in other applications where geometric tolerancing and surface quality are not the most critical aspects, the hot embossing parts may become feasible substitutes. Moreover, these parts can subsequently follow the same finishing done on a bulk metallic mould, namely using EBMa.

We could argue that instead of using hot embossing parts, one can directly use the original metallic mould. But the cost of the original mould is considerably high, and replacing it with the same one would incur in high expenses. It means that for small series and applications where there is not a demand for high dimensional accuracy, its replacement by the same machined mould may not be economically compelling. That said, it is pertinent to assess the final application of a part before deciding which technology one should use.

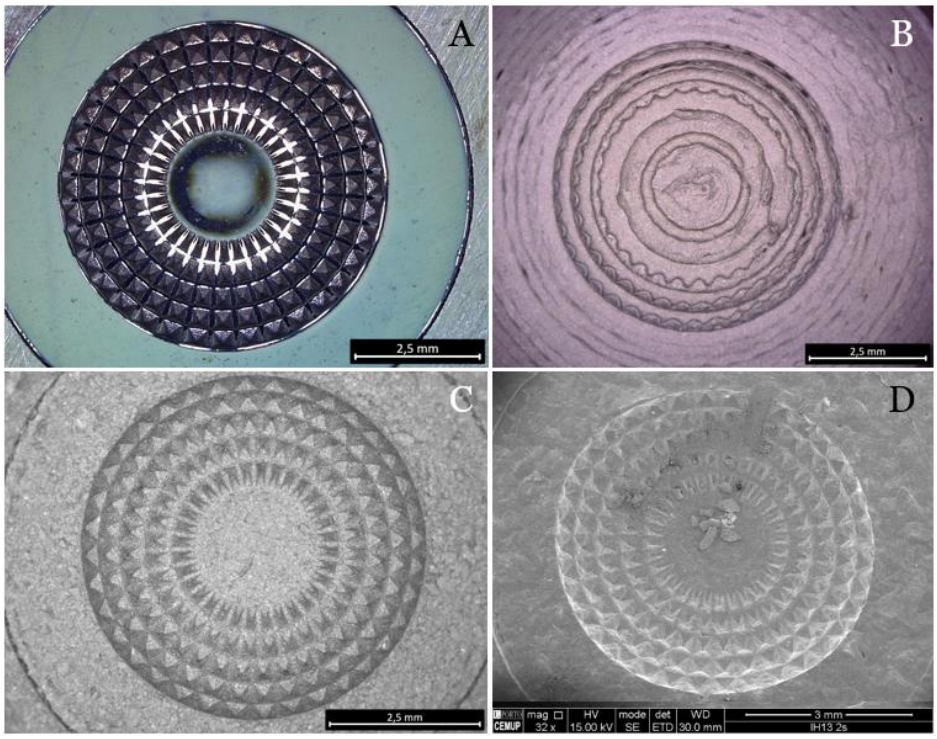

Figure 42: A) Original metallic mould, sintered parts from B) AM, C) hot embossing of the filament and D) hot embossing of SAE H13:M1.

5. Conclusions

In this work, several temperatures, pressures and holding time conditions were under study in the hot embossing of two mixtures. It was found that for the SAE H13:M1 mixture, an increase of 15 minutes in holding time in relation to the initial conditions (220 ºC, 8 MPa, 30 minutes) produced the best results in parts replication. Although the component after sintering shows an acceptable surface appearance, in terms of the microdetails, it has a lot of porosity and large cracks.

As for the hot embossing of the filament, after studying the conditions using a DOE and evaluating the deviations of the components from the silicone rubber die, the best replication results were obtained under the following condition: 210 ºC, 8 MPa, 30 minutes. In this DOE, the temperature was revealed as the determining factor in the quality of replication details. After sintering, the component presented an acceptable replication. Despite not having cracks in its microstructure, the component still displayed considerable porosity like the SAE H13:M1 component. In both cases, the hot embossing part's hardness yielded values around 300 $HV_{0.01}$. In addition, we can conclude that the particle morphology played a significant role during sintering.

Unfortunately, the replication success in hot embossing did not spread to the component produced by extrusion material. The reduced dimensions of the details exposed the limitation of this particular AM technology: the resolution. So at least for now, it is safe to say that AM does not threaten the research around the hot embossing of metallic powders.

Regarding the mechanical properties, all parts improved their hardness after heat treatment. The hardness of the samples sintered in the *Sinter-1* (484 HV0.01) furnace was undoubtedly higher than those in other furnaces. This observation allows us to assert the following premise: a tailored thermal cycle is crucial to obtaining components with the desired mechanical properties.

Based on the results obtained in this work, we acknowledge that hot embossing is a technology with the potential to manufacture components with some intricate microdetails. However, the testing and optimisation of the parameters are crucial to define the adequate processing window to yield the best results in terms of replication.

References

[1] M. Moshiri, D. Loaldi, F. Zanini, D. Sgaravato, S. Carmignato, G. Tosello, Analysis of an as-built metal additively manufactured tool cavity insert performance and advantages for plastic injection moulding, J Manuf Process. 61 (2021) 369–382. https://doi.org/10.1016/j.jmapro.2020.11.035.

[2] D.L. Henann, V. Srivastava, H.K. Taylor, M.R. Hale, D.E. Hardt, L. Anand, Metallic glasses: Viable tool materials for the production of surface microstructures in amorphous polymers by micro-hot-embossing, Journal of Micromechanics and Microengineering. 19 (2009). https://doi.org/10.1088/0960-1317/19/11/115030.

[3] R. Thümmler, F. Oberacker, Introduction to Powder Metallurgy, Maney Publishing for IOM3, the Institute of Materials, Minerals and Mining, 1993. https://app.knovel.com/hotlink/toc/id:kpIPM00015/introduction-powder-metallurgy/introduction-powder-metallurgy.

[4] M. Sahli, J.C. Gelin, Development of a feedstock formulation based on polypropylene for micro-powder soft embossing process of 316L stainless steel micro-channel part, International Journal of Advanced Manufacturing Technology. 69 (2013) 2139–2148. https://doi.org/10.1007/s00170-013-5170-z.

[5] M. Worgull, Introduction, Hot Embossing. (2009) 1–12. https://doi.org/10.1016/B978-0-8155-1579-1.50007-0.

[6] M. Worgull, J.F. Hétu, K.K. Kabanemi, M. Heckele, Modeling and optimization of the hot embossing process for micro- and nanocomponent fabrication, Microsystem Technologies. 12 (2006) 947–952. https://doi.org/10.1007/s00542-006-0124-0.

[7] M. Sahli, J.C. Gelin, T. Barriere, Characterisation and replication of metallic micro-fluidic devices using three different powders processed by hot embossing, Powder Technol. 246 (2013) 284–302. https://doi.org/10.1016/J.POWTEC.2013.05.026.

[8] E.W. Sequeiros, O. Emadinia, M.T. Vieira, M.F. Vieira, Development of metal powder hot embossing: A new method for micromanufacturing, Metals (Basel). 10 (2020). https://doi.org/10.3390/met10030388.

[9] O. Emadinia, M.T. Vieira, M.F. Vieira, Feedstocks of aluminum and 316L stainless steel powders for micro hot embossing, Metals (Basel). 8 (2018). https://doi.org/10.3390/met8120999.

[10] R. Supati, N.H. Loh, K.A. Khor, S.B. Tor, Mixing and characterization of feedstock for powder injection molding, Mater Lett. 46 (2000) 109–114. https://doi.org/10.1016/S0167-577X(00)00151-8.

[11] A.M.O.H. Narasimhan K.S., Powder Characterization, In Reference Module in Materials Science and Materials Engineering. (2017) 1–10. https://doi.org/10.1016/B978-0-12-803581-8.10141-9.

[12] A. Bose, Introduction to Metal Powder Injection Molding, Powder Metallurgy. (2018) 823–847. https://doi.org/10.31399/asm.hb.v07.a0006141.

[13] S. Banerjee, C.J. Joens, Debinding and sintering of metal injection molding (MIM) components, Handbook of Metal Injection Molding. (2012) 133–180. https://doi.org/10.1533/9780857096234.1.133.

[14] J. Zhang, M. Sahli, J.C. Gelin, T. Barriere, Rapid replication of metal microstructures using micro-powder hot embossing process, International Journal of Advanced Manufacturing Technology. 77 (2015) 2135–2149. https://doi.org/10.1007/s00170-014-6595-8.

[15] M. Ouederni, Polymers in textiles, 2020. https://doi.org/10.1016/b978-0-12-816808-0.00010-x.

[16] J. Zhang, J.-C. Gelin, M. Sahli, T. Barriere, Manufacturing of 316L Stainless Steel Die Mold by Hot Embossing Process for Microfluidic Applications, (2013). https://doi.org/10.1115/1.4025554.

[17] M. Sahli, C. Millot, J.C. Gelin, T. Barrière, Development and characterization of polymers-metallic hot embossing process for manufacturing metallic micro-parts, AIP Conf Proc. 1315 (2010) 677–682. https://doi.org/10.1063/1.3552526.

[18] M. Sahli, C. Millot, J.C. Gelin, T. Barrière, The manufacturing and replication of microfluidic mould inserts by the hot embossing process, J Mater Process Technol. 213 (2013) 913–925. https://doi.org/10.1016/j.jmatprotec.2012.11.007.

[19] M. Sahli, J.C. Gelin, T. Barrière, Replication of microchannel structures in WC-Co feedstock using elastomeric replica moulds by hot embossing process, Materials Science and Engineering C. 55 (2015) 252–266. https://doi.org/10.1016/J.MSEC.2015.05.019.

[20] E.W. Sequeiros, Microfabricação de Componentes Metálicos por Microgravação, PhD thesis, University of Porto, 2014. https://hdl.handle.net/10216/75061.

[21] G. Fu, S.B. Tor, N.H. Loh, D.E. Hardt, Micro-hot-embossing of 316L stainless steel micro-structures, Appl Phys A Mater Sci Process. 97 (2009) 925–931. https://doi.org/10.1007/s00339-009-5363-3.

[22] E.W. Sequeiros, V.C. Neto, M.T. Vieira, M.F. Vieira, Powder Metallurgy Hot micro-embossing: effect of pressure on 316L metal parts, (2014). https://doi.org/10.1179/0032589914Z.000000000193.

[23] E.M. Cahill, S. Keaveney, V. Stuettgen, P. Eberts, P. Ramos-Luna, N. Zhang, M. Dangol, E.D. O'Cearbhaill, Metallic microneedles with interconnected porosity: A scalable platform for biosensing and drug delivery, Acta Biomater. 80 (2018) 401–411. https://doi.org/10.1016/j.actbio.2018.09.007.

[24] O. Emadinia, Micro hot embossing of metallic reinforced powders, PhD thesis, University of Porto, 2018.

[25] I. Todd, A.T. Sidambe Dr, Developments in metal injection moulding (MIM), 2013. https://doi.org/10.1533/9780857098900.1.109.

[26] U. Anselmi-Tamburini, Spark plasma sintering, Encyclopedia of Materials: Technical Ceramics and Glasses. 1–3 (2021) 294–310. https://doi.org/10.1016/B978-0-12-803581-8.11730-8.

[27] S.H. Choi, S.D. Kang, Y.S. Kwon, S.G. Lim, K.K. Cho, I.S. Ahn, The effect of sintering conditions on the properties of WC-10wt%Co PIM compacts, Research on Chemical Intermediates. 36 (2010) 743–748. https://doi.org/10.1007/s11164-010-0176-8.

[28] N. Zhang, A. Srivastava, B. Kirwan, R. Byrne, F. Fang, D.J. Browne, M.D. Gilchrist, Manufacturing microstructured tool inserts for the production of polymeric microfluidic devices, Journal of Micromechanics and Microengineering. 25 (2015). https://doi.org/10.1088/0960-1317/25/9/095005.

[29] F. Biondani, G. Bissacco, P.T. Tang, H.N. Hansen, Additive Manufacturing of Mould Inserts with Mirror-like Surfaces, Procedia CIRP. 68 (2018) 369–374. https://doi.org/10.1016/j.procir.2017.12.097.

[30] J.M. Torralba, M. Campos, High entropy alloys manufactured by additive manufacturing, Metals (Basel). 10 (2020) 1–15. https://doi.org/10.3390/met10050639.

[31] J.M. Torralba, P. Alvaredo, A. García-Junceda, High-entropy alloys fabricated via powder metallurgy. A critical review, Powder Metallurgy. 62 (2019) 84–114. https://doi.org/10.1080/00325899.2019.1584454.

[32] M. Molitch-Hou, Overview of additive manufacturing process, in: Addit Manuf, Elsevier, 2018: pp. 1–38. https://doi.org/10.1016/B978-0-12-812155-9.00001-3.

[33] L. Zhu, P. Xue, Q. Lan, G. Meng, Y. Ren, Z. Yang, P. Xu, Z. Liu, Recent research and development status of laser cladding: A review, Opt Laser Technol. 138 (2021) 106915. https://doi.org/10.1016/j.optlastec.2021.106915.

[34] C.Y. Yap, C.K. Chua, Z.L. Dong, Z.H. Liu, D.Q. Zhang, L.E. Loh, S.L. Sing, Review of selective laser melting: Materials and applications, Appl Phys Rev. 2 (2015). https://doi.org/10.1063/1.4935926.

[35] L.E. Murr, S.M. Gaytan, Electron Beam Melting, Elsevier, 2014. https://doi.org/10.1016/B978-0-08-096532-1.01004-9.

[36] R. Stolt, A.E.W. Jarfors, Manufacturing of High Pressure Die Casting Die Inserts Using SLM, Advances in Transdisciplinary Engineering. 13 (2020) 663–671. https://doi.org/10.3233/ATDE200206.

[37] R. Leal, F.M. Barreiros, L. Alves, F. Romeiro, J.C. Vasco, M. Santos, C. Marto, Additive manufacturing tooling for the automotive industry, International Journal of Advanced Manufacturing Technology. 92 (2017) 1671–1676. https://doi.org/10.1007/s00170-017-0239-8.

[38] G. Bi, G.K.L. Ng, K.M. Teh, A.E.W. Jarfors, Feasibility study on the Laser Aided Additive Manufacturing of die inserts for liquid forging, Mater Des. 31 (2010) S112–S116. https://doi.org/10.1016/j.matdes.2009.10.039.

[39] D.M. Santhoshsarang, K. Divya, G. Telasang, S. Soundarapandian, R. Bathe, G. Padmanabham, Additively Manufactured High-Performance Conformally Cooled H13 Tool Steel Die Insert for Pressure Die Casting, Transactions of the Indian National Academy of Engineering. 6 (2021) 1037–1048. https://doi.org/10.1007/s41403-021-00233-y.

[40] B. Reggiani, I. Todaro, Investigation on the design of a novel selective laser melted insert for extrusion dies with conformal cooling channels, International Journal of

Advanced Manufacturing Technology. 104 (2019) 815–830. https://doi.org/10.1007/s00170-019-03879-9.

[41] L.E. Rannar, A. Glad, C.G. Gustafson, Efficient cooling with tool inserts manufactured by electron beam melting, Rapid Prototyp J. 13 (2007) 128–135. https://doi.org/10.1108/13552540710750870.

[42] M.A. Wagner, A. Hadian, T. Sebastian, F. Clemens, T. Schweizer, M. Rodriguez-Arbaizar, E. Carreño-Morelli, R. Spolenak, Fused filament fabrication of stainless steel structures - from binder development to sintered properties, Addit Manuf. 49 (2022) 102472. https://doi.org/10.1016/J.ADDMA.2021.102472.

[43] H. Ma, Y. Zhang, Z. Jiao, W. Yang, X. He, G. Xie, H. Li, Comprehensive Assessment of the Environmental Impact of Fused Filament Fabrication Products Produced Under Various Performance Requirements, Journal of The Institution of Engineers (India): Series C. 102 (2021) 59–73. https://doi.org/10.1007/S40032-020-00637-9/FIGURES/11.

[44] G. Wu, N.A. Langrana, R. Sadanji, S. Danforth, Solid freeform fabrication of metal components using fused deposition of metals, Mater Des. 23 (2002) 97–105. https://doi.org/10.1016/S0261-3069(01)00079-6.

[45] M.Q. Shaikh, P.Y. Lavertu, K.H. Kate, S. v. Atre, Process Sensitivity and Significant Parameters Investigation in Metal Fused Filament Fabrication of Ti-6Al-4V, J Mater Eng Perform. 30 (2021) 5118–5134. https://doi.org/10.1007/s11665-021-05666-8.

[46] E.B. Fonseca, A.H.G. Gabriel, L.C. Araújo, P.L.L. Santos, K.N. Campo, E.S.N. Lopes, Assessment of laser power and scan speed influence on microstructural features and consolidation of AISI H13 tool steel processed by additive manufacturing, Addit Manuf. 34 (2020) 101250. https://doi.org/10.1016/J.ADDMA.2020.101250.

[47] J.M.Costa, E.W.Sequeiros, M.T.Vieira, M.F.Vieira, Additive Manufacturing: Material Extrusion of Metallic Parts, Submitted to the Journal U.Porto Journal of Engineering; ISSN 2183-6493; 2 (2021) 53–69. https://doi.org/10.24840/2183-6493_007.003_0005.

[48] I. Buj-Corral, A. Tejo-Otero, F. Fenollosa-Artés, Development of am technologies for metals in the sector of medical implants, Metals (Basel). 10 (2020) 1–31. https://doi.org/10.3390/met10050686.

[49] W.E. Bryson, 30.12 H13 Tool Steel, in: Heat Treatment - Master Control Manual, Hanser Publishers, 2015: pp. 201–253. https://app.knovel.com/hotlink/pdf/id:kt010RRZU2/heat-treatment-master/h13-tool-steel.

[50] Markforged, H13 Tool Steel, Material Datasheet. (2018) 1. http://www.astmsteel.com/product/h13-tool-steel-x40crmov5-1-skd61-hot-work-steel/.

[51] E.W. Sequeiros, M.T. Vieira, M.F. Vieira, Micro metal powder hot embossing: influence of binder on austenitic stainless steel microparts replicability, (2021). https://doi.org/10.1080/00325899.2021.1952514.

[52] F. Chu, K. Zhang, H. Shen, M. Liu, W. Huang, X. Zhang, E. Liang, Z. Zhou, L. Lei, J. Hou, A. Huang, Influence of satellite and agglomeration of powder on the processability of AlSi10Mg powder in Laser Powder Bed Fusion, Journal of Materials

Research and Technology. 11 (2021) 2059–2073. https://doi.org/10.1016/J.JMRT.2021.02.015.

[53] M.J. Desroches, I.A. Castillo, R.J. Munz, Determination of particle size distribution by laser diffraction of doped-CeO2 powder suspensions: Effect of suspension stability and sonication, Particle and Particle Systems Characterization. 22 (2006) 310–319. https://doi.org/10.1002/ppsc.200500996.

[54] J. Damon, S. Dietrich, S. Gorantla, U. Popp, B. Okolo, V. Schulze, Process porosity and mechanical performance of fused filament fabricated 316L stainless steel, Rapid Prototyp J. 25 (2019) 1319–1327. https://doi.org/10.1108/RPJ-01-2019-0002.

[55] B. Zhang, F. Yang, Q. Qin, T. Lu, H. Sun, S. Lin, C. Chen, Z. Guo, Characterisation of powder metallurgy H13 steels prepared from water atomised powders, Powder Metallurgy. 63 (2020) 9–18. https://doi.org/10.1080/00325899.2019.1692169.

[56] M. Blair, Specialty Steels and Heat-Resistant Alloys, Cast Stainless Steels, Metals Handbook, Volume 1. (1990) 908–929. https://doi.org/10.1361/asmhba0001.

[57] ASM International, Heat Treating of Steel, Metals Handbook Desk Edition. (1991) 970–982. https://doi.org/10.31399/asm.hb.mhde2.a0003196.

[58] P.B. Hopper, Heat treatment of tool steels, SME Technical Paper (Series) CM. (1993) 1–13. https://doi.org/10.31399/asm.tb.phtbp.t59310285.

[59] R.P. Koseski, P. Suri, N.B. Earhardt, R.M. German, Y.S. Kwon, Microstructural evolution of injection molded gas- and water-atomized 316L stainless steel powder during sintering, Materials Science and Engineering A. 390 (2005) 171–177. https://doi.org/10.1016/J.MSEA.2004.08.002.

[60] V. Rudnev, D. Loveless, R.L. Cook, Industrial Applications of Induction Heating, Handbook of Induction Heating. (2017) 9–50. https://doi.org/10.1201/9781315117485-2.

Appendix I

In this work, we tested three different ways to disaggregate the filament: manual milling with a mortar, grinding with a coffee grinder and manual crushing with a hammer. Looking at the Figure 43, the obtained granulates does not display considerable differences. So, the coffee grinding methodology seems the way to go to reduce the labour intensity from a manual mortar milling or hammer crushing.

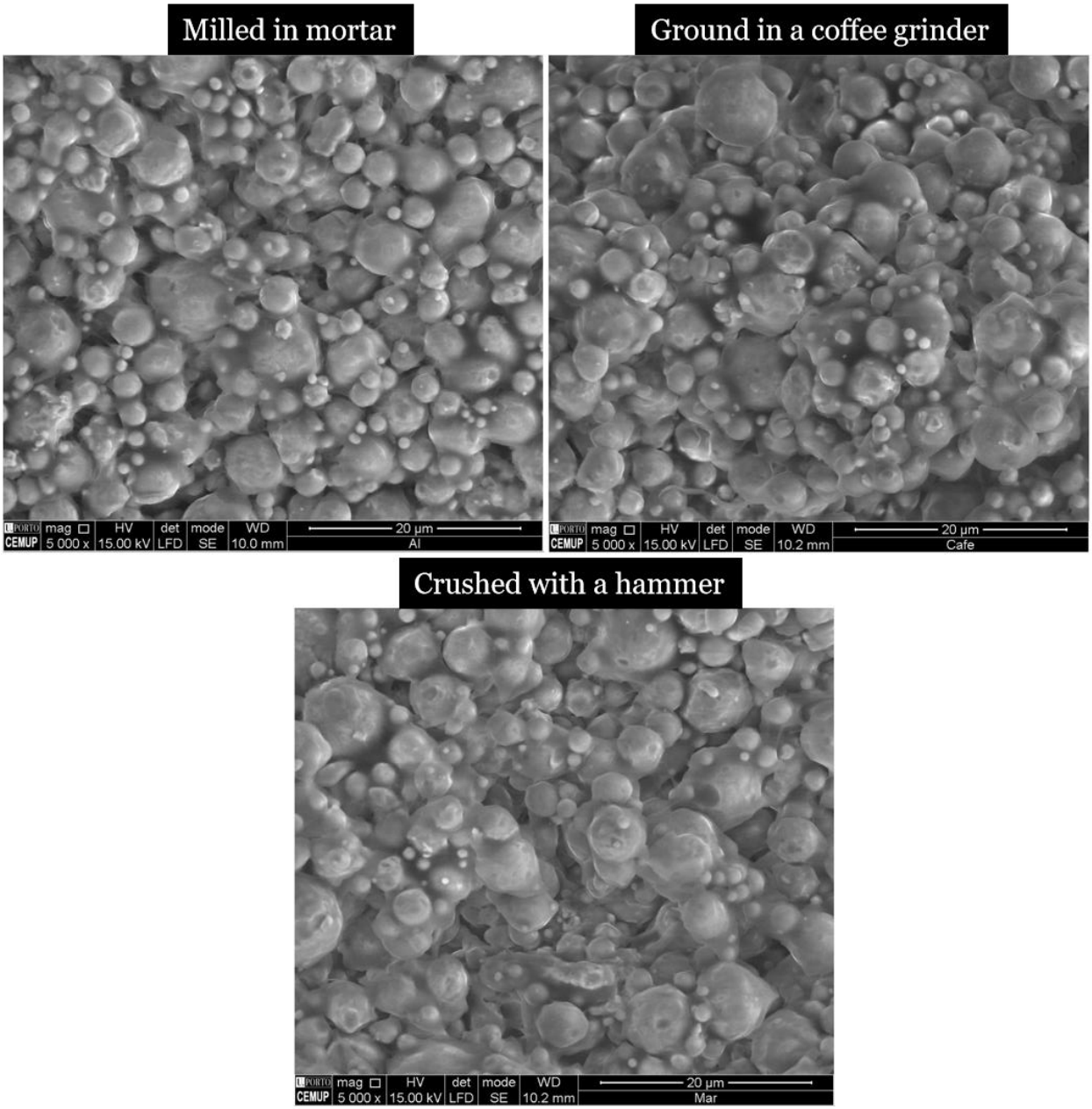

Figure 43: SAE H13 filament disaggregated in three different ways.